

September 30, 2019

Dear Editor,

We have received the comments from the two reviewers of the manuscript. Below are our responses and the revisions that we have made in the manuscript.

Thank you for your efforts on this manuscript. We look forward to hearing from you.

Best Regards,

Guohui Li

Reply to Anonymous Referee #1

We thank the reviewer for the careful reading of the manuscript and helpful comments. We have revised the manuscript following the suggestion, as described below.

Liu et al. presented a regional modeling study about the effects of stabilized Criegee Intermediates (sCI) on sulfate formation during the summertime in Beijing-Tianjin-Hebei, China. They found that the heterogeneous uptake involving aerosol water and gas-phase OH oxidation of SO₂ were the two important source of sulfate, while sCI oxidation pathway could be insignificant in the actual case. This study calls for the attention of a better-constrained evaluation of the role of sCI in sulfate formation in regional and global models. This manuscript is overall well-written and the discussion is sound. I recommend for publication after considering the following points:

General comments:

1. About heterogeneous oxidation: It is better to show some more details about this reaction pathway since it is the most important contribution but only one parameter (γ) is involved. For example, how much is the aerosol-phase liquid water content in the model during this period? What is the total surface area of particles? What are the fractions that POA and SOA contributing to heterogeneous oxidation of SO₂? How about the sensitivity test of γ to sCI contribution?

Response: We have clarified in Section 2.2: *“The aerosol hygroscopic growth is directly predicted by ISORROPIA in the model, and the aerosol water surface area is scaled from the calculated wet aerosol surface area using the third-moment of aerosol species.”*

We have clarified in Section 3.3: *“It is worth noting that the uncertainty in HR_SO₂, as the most important sulfate source, also influences the sulfate contribution of sCI_SO₂. Several factors influence the heterogeneous reactions of SO₂ on aerosol*

surfaces, including aerosol water surface area, aerosol acidity, organic coating, et al. In the B-case, the predicted average aerosol liquid water and wet surface area are $18.8 \mu\text{g m}^{-3}$ and $2.4 \times 10^{-4} \text{ m}^2 \text{ m}^{-3}$ in the BTH during the episode, and the uptake coefficient of SO_2 by aerosols (γ) is assumed as 0.5×10^{-4} . To investigate the sensitivity of $s\text{CI}_{\text{SO}_2}$ sulfate contributions to uncertainties in HR_{SO_2} , we perform sensitivity simulations with γ of 0.25×10^{-4} and 1.0×10^{-4} . The sulfate concentration of HR_{SO_2} is affected considerably by the variation of γ , with the average change of -18.3% and 25.6% in BTH during the episode when the γ is assumed as 0.25×10^{-4} and 1.0×10^{-4} , respectively. However, effects of the γ change to sulfate contributions of $s\text{CI}_{\text{SO}_2}$ is not significant, with the change of -4.4% and 3.9% when the γ is assumed as 0.25×10^{-4} and 1.0×10^{-4} , respectively.”

2. About sCI profile: The authors only showed the sCI effect of SO_2 . What are the temporal profiles of sCIs? How about the fates of them in the atmosphere, especially for different sCI types? Is H_2O always the predominant sink of sCIs?

Response: We have clarified in Section 3.3: “Figure 10 shows the diurnal profiles of $s\text{CI}_1$, $s\text{CI}_2$ and $s\text{CI}_3$ concentrations in BTH from 04 to 15 July 2015. The average concentration of $s\text{CI}_1$, $s\text{CI}_2$ and $s\text{CI}_3$ is 1.8×10^4 , 2.0×10^4 and 1.9×10^4 molecules cm^{-3} , respectively. Novelli et al. (2017) have estimated the concentration of sCI in the lower troposphere based on the observation in a boreal forest in Finland and in rural southern Germany. The results show that the average concentration of sCI is about 5.0×10^4 molecules cm^{-3} , with an order of magnitude uncertainty, generally consistent with our study. Dominant sCI peaks frequently occur during nighttime, mainly caused by the low PBL facilitating accumulation of alkenes and sCI and low reaction rates of sCI with other species (Smith et al., 2015; Stone et al., 2014; Taatjes et al., 2017). It is worth noting that sCI are predominantly quenched by reactions with water vapor in the atmosphere.”

Specific comments:

1. Page 2 Line 62: "Basing on" should be "based on"

Response: We have changed “Basing on” to “Based on” in the sentence.

2. Page 11 Line 282: "worth nothing..." should be "worth noting"

Response: We have revised “worth nothing” to “worth noting” in the sentence.

3. Figure 4: the legend for wind speed is too small

Response: We have revised the legend of wind speed in Figure 4.

4. Figure 9: what could be the potential reasons for the dominant peak of sulfate temporal profile in S1 and S2 cases around July 10, while in other time periods much smoother and lower compared with the base case?

Response: We have clarified in Section 3.3: *“In the S1-case and S2-case, there is a dominant peak of sulfate concentrations on July 10, which might be caused by the reaction rate constants used in the two cases. We have performed an additional sensitivity study (S3-case), in which the reported κ_{sCI+SO_2} ($3.42 \times 10^{-11} \text{ cm}^3 \text{ s}^{-1}$) and κ_{sCI+H_2O} ($7.4 \times 10^{-12} \text{ cm}^3 \text{ s}^{-1}$) suggested by Stone et al. (2014) and Smith et al. (2015) are used. The results show that the average sulfate contribution of sCI_SO_2 becomes more insignificant, about $0.06 \mu\text{g m}^{-3}$ or less than 0.6%. However, there is no obvious peak around July 10 (Figure 11), indicating that the large uncertainty in contributions of sCI_SO_2 to sulfate mass is due to the different value of κ_{sCI+SO_2} and κ_{sCI+H_2O} used in the sensitivity studies.”*

References:

- Novelli, A., Hens, K., Tatum Ernest, C., Martinez, M., Nölscher, A. C., Sinha, V., Paasonen, P., Petäjä, T., Sipilä, M., Elste, T., Plass-Dülmer, C., Phillips, G. J., Kubistin, D., Williams, J., Vereecken, L., Lelieveld, J., and Harder, H.: Estimating the atmospheric concentration of Criegee intermediates and their possible interference in a FAGE-LIF instrument, *Atmos. Chem. Phys.*, 17, 7807–7826, <https://doi.org/10.5194/acp-17-7807-2017>, 2017.
- Smith, M., Chang, C-H., Chao, W., Lin, L-C., Takahashi, K., Boering, K., and Lin, J. J-M: Strong negative temperature dependence of the simplest Criegee Intermediate CH_2OO reaction with water dimer, *J. Phys. Chem. Lett.*, 6(14), 2708–2713, <https://doi.org/10.1021/acs.jpcclett.5b01109>, 2015.

- Stone, D., Blitz, M., Daubney, L., Howes, N., and Seakins, P.: Kinetics of CH₂OO reactions with SO₂, NO₂, NO, H₂O and CH₃CHO as a function of pressure, *Phys. Chem. Chem. Phys.*, 16, 1139–1149, <https://doi.org/10.1039/c3cp54391a>, 2014.
- Taatjes, C. A.: Criegee intermediates: What direct production and detection can teach us about reactions of carbonyl oxides, *Annu. Rev. Phys. Chem.* 2017. 68:183–207, <https://doi.org/10.1146/annurev-physchem-052516-050739>, 2017.

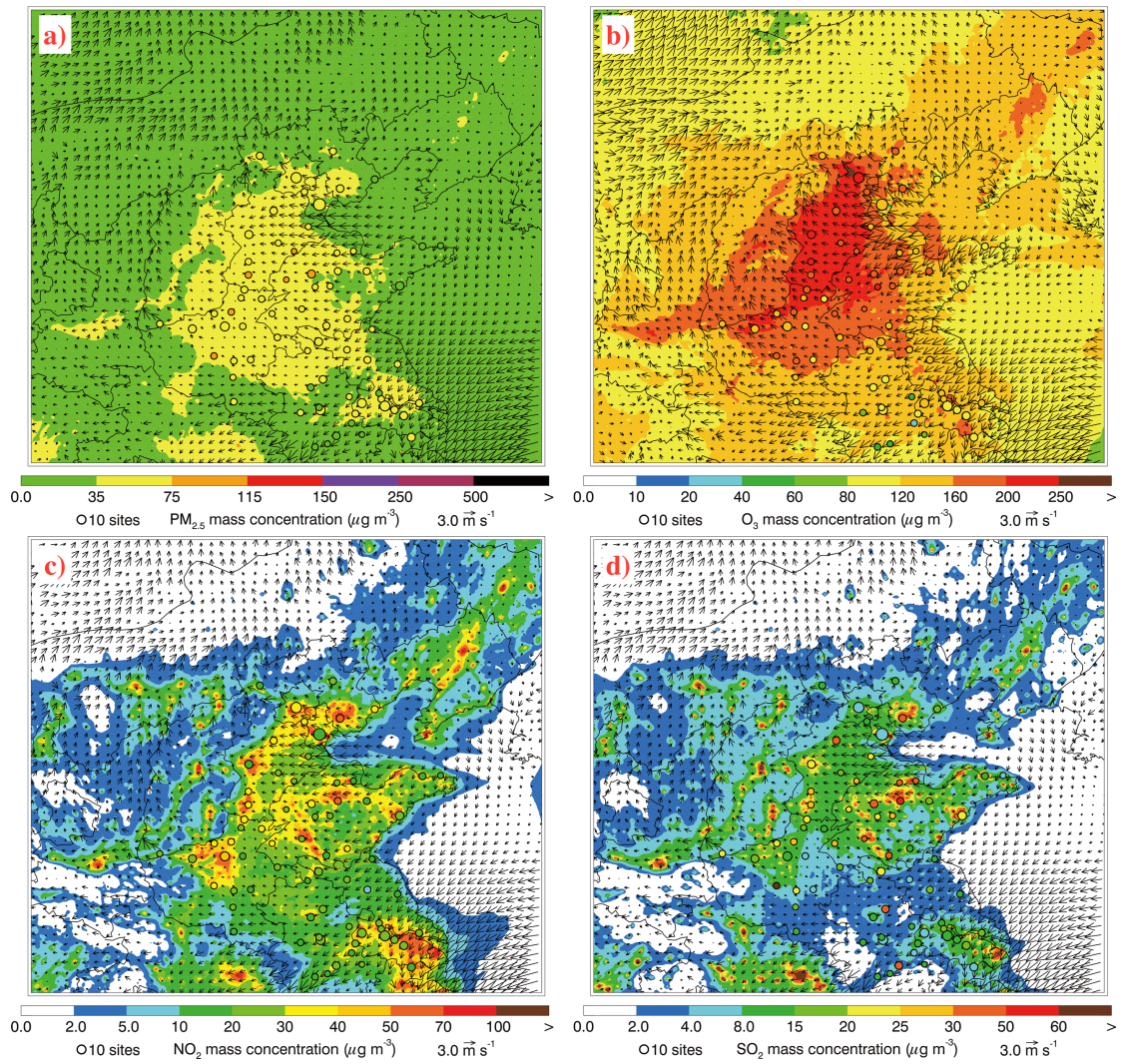


Figure 4 Spatial distributions of average (a) PM_{2.5}, (b) peak O₃, (c) NO₂, and (d) SO₂ mass concentrations from 04 to 15 July 2015. Colored dots, colored contour, and black arrows are observations and simulations of air pollutants, and simulated surface winds, respectively.

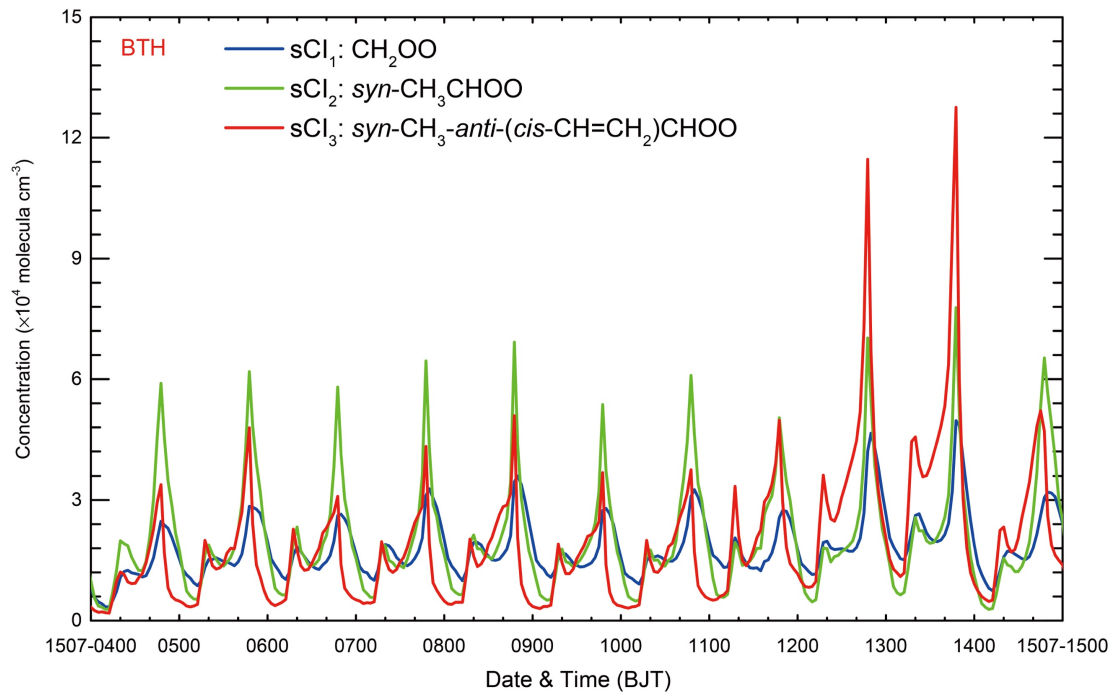


Figure 10 Temporal variations of the average simulated concentration of different sCI (Blue line: sCI₁; Green line: sCI₂; Red line: sCI₃) in BTH from 04 to 15 July 2015.

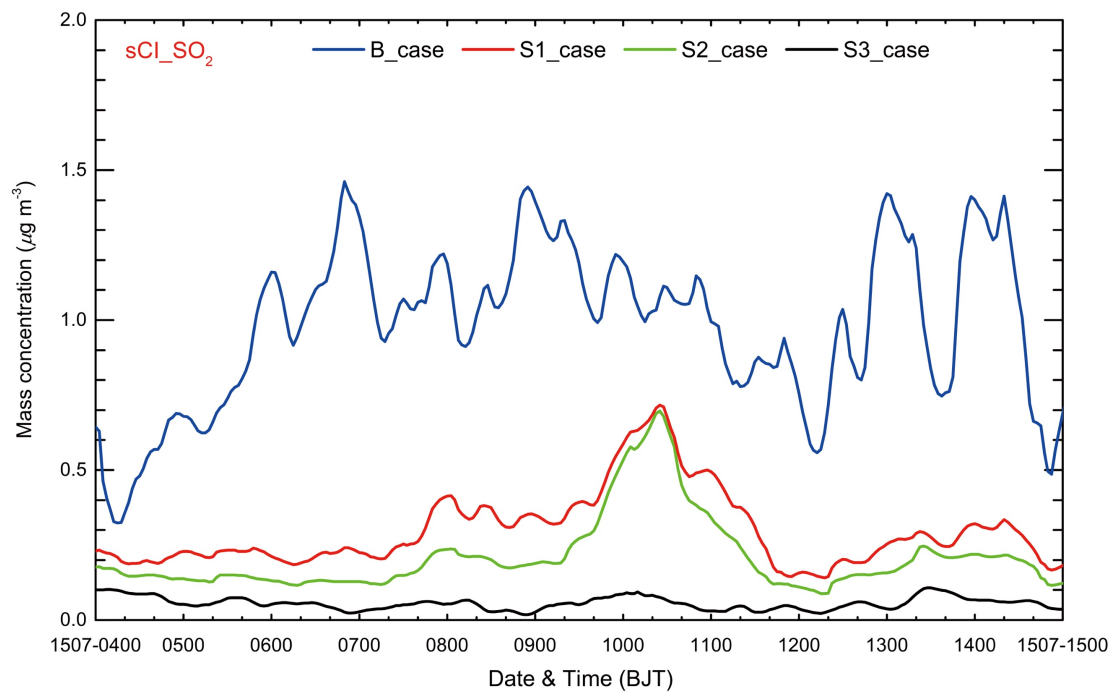


Figure 11 Temporal variations of the simulated average sulfate concentration contributed by the sCl_SO₂ (Blue line: B-case; Red line: S1-case; Green line: S2-case; Black line: S3-case) in BTH from 04 to 15 July 2015.

Reply to Anonymous Referee #3

This manuscript presents a modeling study to quantify the contribution of stabilized Criegee Intermediates (sCI) on the sulfate formation in the BTH region using a source-oriented WRF-Chem model. The topic is well within the ACP domain and is well addressed, the methodology is sound, and the results are well presented. The work can be accepted for publishing after the following minor issues are addressed.

1 Comment: The authors use the results of the sCI contribution on the sulfate formation at one station (NCNST) to draw a general conclusion in the BTH. This is a bit of overstretch. It needs to be clarified. Besides the results at the NCNST site, it would be valuable to select a larger source area and a downwind area to discuss the contributions of the sCI and other three pathways. With this expansion, the paper would present a more general picture of the sulfate sources in the BTH.

Response: We have clarified in Section 3.2: *“Figures 8b-e present the simulated temporal variations of the four pathways to the sulfate concentration averaged over the whole BTH from 04 to 15 July 2015. On average, the HR_SO₂ is still the dominant sulfate source, with a contribution of 35.3% (Figure 8b). The OH_SO₂ plays an important role in the sulfate formation, accounting for 33.1% of sulfate mass (Figure 8c). The primary emission pathway and sCI_SO₂ contributes 22.5% and 9.1% of the sulfate concentration, respectively (Figures 8d and 8e).”*

2 Comment: Regard the effects of sCI on the sulfate formation, in addition to the oxidation of SO₂ by sCI, sCI may also contribute to the sulfate formation through enhancing the atmospheric oxidation capacity, since sCI may enhance the ozone formation and ultimately enhance OH, and thus enhance the SO₂ oxidation by OH. The latter can be called the indirect effects by sCI. It would be helpful to evaluate the sCI's indirect effects.

Response: We have clarified in Section 4: *“Additionally, as a potentially important atmospheric oxidant, sCI may enhance ozone formation and ultimately the OH formation. The indirect effects of sCI on the sulfate formation by promoting the OH-SO₂ pathway should also be investigated further.”*

3 Comment: Not considering the aqueous SO₂ oxidation in cloud or fog droplets on one hand may underestimate the sulfate formation, and on the other hand may overestimate the contributions from other sources, including the sCI source.

Response: We have clarified in Section 2.2: *“It is worth noting that the WRF-Chem model cannot well resolve clouds formed in the planetary boundary layer (PBL), so the aqueous SO₂ oxidation in cloud or fog droplets is not considered in the study, which might cause the sulfate underestimation, and on the other hand might overestimate the contributions of the four pathways to the sulfate concentration.”*

4 Comment: There is no information on emission inventory used in the simulation.

Response: We have clarified in Section 2.1: *“The anthropogenic emission inventory with a horizontal resolution of 6km is developed by Zhang et al. (2009), with the base year of 2013, including industry, transportation, power plant, residential and agriculture sources. The Model of Emissions of Gases and Aerosols from Nature (MEGAN) is used to calculate the biogenic emissions online (Guenther et al., 2006).”*

5 Comment: In the abstract, the statement “The primary emission accounts for around 22~24% of sulfate concentrations due to high SO₂ emissions” is confusing. Is this due to the sulfate emissions and due to the SO₂ emissions?

Response: We have revised the sentence in the abstract: *“The primary sulfate emission accounts for around 22~24% of the total sulfate concentration.”*

References:

Guenther, A., Karl, T., Harley, P., Wiedinmyer, C., Palmer, P. I., and Geron, C.: Estimates of global terrestrial isoprene emissions using MEGAN (Model of Emissions of Gases and Aerosols from Nature), *Atmos. Chem. Phys.*, 6, 3181–3210, <https://doi.org/10.5194/acp-6-3181-2006>, 2006.

Zhang, Q., Streets, D. G., Carmichael, G. R., He, K., Huo, H., Kannari, A., Klimont, Z., Park, I. S., Reddy, S., Fu, J., Chen, D., Duan, L., Lei, Y., Wang, L., and Yao, Z.: Asian emissions in 2006 for the NASA INTEX-B mission, *Atmos. Chem. Phys.*, 9, 5131–5153, <https://doi.org/10.5194/acp-9-5131-2009>, 2009.

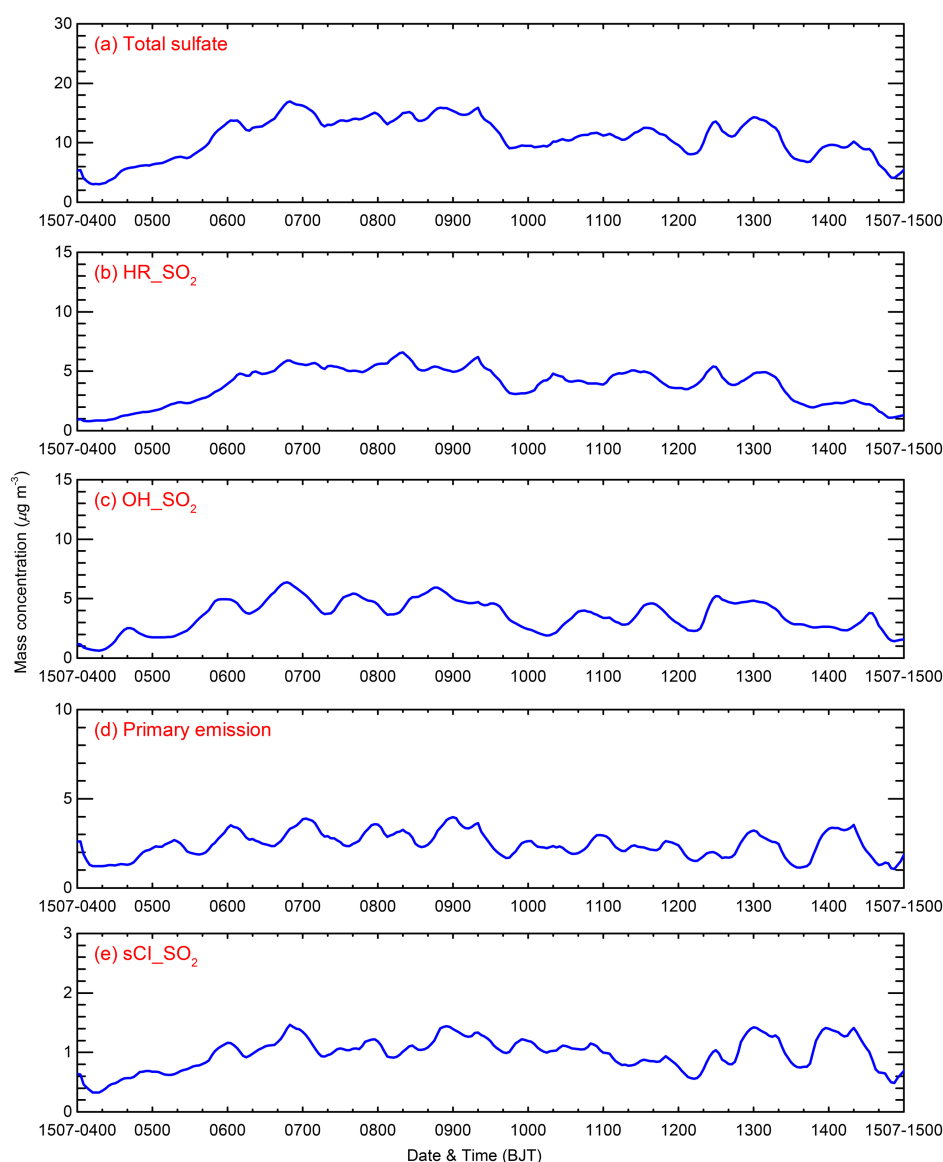


Figure 8 (a) Simulated diurnal profiles of total sulfate mass concentration, and contributions of the (b) HR_SO₂, (c) OH_SO₂, (d) primary emission, and (e) sCl_SO₂ to the sulfate concentration averaged over BTH from 04 to 15 July 2015.

1 Effects of stabilized Criegee Intermediates (sCI) on the sulfate formation: A sensitivity
2 analysis during summertime in Beijing-Tianjin-Hebei (BTH), China

3
4 Lang Liu^{1,3,4}, Naifang Bei², Jiarui Wu^{1,3}, Suixin Liu^{1,3}, Jiamao Zhou^{1,3}, Xia Li^{1,3}, Qingchuan Yang¹, Tian Feng¹,
5 Junji Cao^{1,3}, Xuexi Tie¹, Guohui Li^{1,3*}

6
7 ¹Key Lab of Aerosol Chemistry and Physics, SKLLQG, Institute of Earth Environment, Chinese Academy of
8 Sciences, Xi'an, 710061, China

9 ²School of Human Settlements and Civil Engineering, Xi'an Jiaotong University, Xi'an, Shaanxi, 710049,
10 China

11 ³CAS Center for Excellence in Quaternary Science and Global Change, Xi'an, 710061, China

12 ⁴University of Chinese Academy of Sciences, Beijing, 100049, China

13
14 *Correspondence to:* Guohui Li (ligh@ieecas.cn)

15
16 **Abstract:** Sulfate aerosols exert profound impacts on climate, ecosystem, visibility, and
17 public health, but the sulfate formation pathway remains elusive. In the present study, a
18 source-oriented WRF-Chem model is applied to simulate a persistent air pollution episode
19 from 04 to 15 July 2015 in Beijing-Tianjin-Hebei (BTH), China to study contributions of four
20 pathways to the sulfate formation. When comparing simulations to measurements in BTH,
21 the index of agreement (IOA) of meteorological parameters, air pollutants and aerosol species
22 generally exceeds 0.6. On average in BTH, the heterogeneous reaction of SO₂ involving
23 aerosol water and the SO₂ oxidation by OH constitutes the two most important sulfate
24 sources, with a contribution of about 35~38% and 33~36% respectively. **The primary sulfate**
25 **emission accounts for around 22~24% of the total sulfate concentration.** The SO₂ oxidation
26 by stabilized Criegee Intermediates (sCI) also plays an appreciable role in the sulfate
27 formation, with a contribution of around 9% when an upper limit of the reaction rate constant
28 of sCI with SO₂ ($\kappa_{sCI+SO_2}=3.9\times 10^{-11}$ cm³ s⁻¹) and a lower limit of the reaction rate constant of
29 sCI with H₂O ($\kappa_{sCI+H_2O}=1.97\times 10^{-18}$ cm³ s⁻¹) are used. Sensitivity studies reveal that there still
30 exist large uncertainties in the sulfate contribution of the SO₂ oxidation by sCI. The sulfate
31 contribution of the reaction is decreased to less than 3% when κ_{sCI+SO_2} is decreased to
32 6.0×10^{-13} cm³ s⁻¹. Furthermore, when κ_{sCI+H_2O} is increased to 2.38×10^{-15} cm³ s⁻¹ based on
33 the reported ratio of κ_{sCI+H_2O} to κ_{sCI+SO_2} (6.1×10^{-5}), the sulfate contribution becomes
34 insignificant, less than 2%. Further studies need to be conducted to better determine κ_{sCI+SO_2}
35 and κ_{sCI+H_2O} to evaluate effects of the sCI chemistry on the sulfate formation.

39 1 Introduction

40 As a major component of fine particulate matters (PM_{2.5}) in the atmosphere, sulfate
41 aerosols not only directly and indirectly influence regional and global climate, also impair
42 ecosystem, visibility and potentially public health (e.g., Wang and Hao, 2012; Guo et al.,
43 2014; Gao et al., 2016; Tao et al., 2017). Sulfate aerosols are primarily formed through
44 homogeneous and heterogeneous oxidations of sulfur dioxide (SO₂) emitted from
45 anthropogenic and natural sources (Seinfeld and Pandis, 2006). The sulfate formation
46 pathway via the SO₂ oxidation includes aqueous reactions in cloud or fog droplets,
47 heterogeneous reactions associated with aerosol water, and gas-phase reactions with hydroxyl
48 radicals (OH) and stabilized Criegee Intermediates (sCI) (Seinfeld and Pandis, 2006; Wang et
49 al., 2016; Li et al., 2017). Recent studies have revealed that the SO₂ oxidation by sCI could
50 constitute an important sulfate source in the atmosphere (Welz et al., 2012; Mauldin et al.,
51 2012; Boy et al., 2013; Pierce et al., 2013; Percival et al., 2013).

52 Carbonyl oxide intermediates formed in the ozonolysis reaction of alkenes, often known
53 as sCI, are proposed to be important radicals in the atmosphere. In the gas phase, sCI can act
54 as an additional atmospheric oxidant. Laboratory studies in the 1970s have shown that the
55 SO₂ oxidation is enhanced in the presence of alkenes and ozone, providing the first evidence
56 that sCI could react with SO₂ (Cox and Penkett, 1971). In the 2010s, Welz et al. (2012) have
57 used photoionization mass spectrometry to make the first direct measurement of individual
58 sCI isomers. They have found that the reaction rate of the simplest sCI, H₂COO, with SO₂ is
59 faster than expected by up to three orders of magnitude, whereas the removal of sCI by water
60 vapor is comparatively slow. The result has also indicated that the sCI chemistry potentially
61 contributes substantially to the SO₂ oxidation, and exerts profound effects on the sulfate
62 formation. **Based** on the laboratory experiments and theoretical considerations, Mauldin et al.
63 (2012) have reported the reaction rate of the sCI originated from the ozonolysis reaction of

64 α -pinene and limonene with SO₂ under boundary layer atmospheric conditions. The new
65 reaction rates are slower than those found in Welz et al. (2012), but still about one order of
66 magnitude faster than previously used (Jenkin et al., 1997).

67 Further studies have been conducted to evaluate contributions of the SO₂ oxidation by
68 sCI to the sulfate in the atmosphere, based on the results of Welz et al. (2012) and Mauldin et
69 al. (2012). Boy et al. (2013) have examined effects of the increased reaction rate of sCI with
70 SO₂ on the atmospheric sulfuric acid (H₂SO₄) concentration at two stations, showing that the
71 reaction contributes as much as 33-46% of H₂SO₄ concentrations at the ground level. Using
72 the results of Welz et al. (2012), Sarwar et al. (2013) have shown that the SO₂ oxidation by
73 sCI does not substantially influence sulfate concentrations in the USA due to the competing
74 reaction of sCI with water vapor. However, when using the high reaction rate constant of sCI
75 with SO₂ (κ_{sCI+SO_2}) and the low reaction rate constant of sCI with H₂O (κ_{sCI+H_2O})
76 simultaneously, the SO₂ oxidation by sCI considerably enhances the sulfate formation
77 (Sarwar et al., 2014). Li et al. (2013) have demonstrated that the SO₂ oxidation by sCI
78 contributes about 18% of the sulfate concentration during summertime in the eastern USA,
79 when using the κ_{sCI+SO_2} reported by Welz et al. (2012). Pierce et al. (2013) have used the
80 same κ_{sCI+SO_2} in simulations of the GEOS-CHEM model, showing that the reaction
81 increases the H₂SO₄ production globally by 4%, and the induced H₂SO₄ enhancement is
82 almost entirely distributed over the forested continental regions with large fluxes of biogenic
83 alkene emissions.

84 With rapid industrialization and urbanization, heavy air pollution with high levels of
85 PM_{2.5} and/or ozone (O₃) frequently occurs in Beijing-Tianjin-Hebei (BTH), and sulfate
86 aerosols have become a main component of PM_{2.5} (e.g., Zhang et al., 2012; Zhao et al., 2013;
87 Sun et al., 2015; Li et al., 2017; Wu et al., 2017). Considering the high alkenes emissions and
88 increasing trend of O₃ concentrations during summertime in BTH, it is imperative to assess

89 effects of the sCI chemistry on the sulfate formation. In the present study, a source-oriented
90 WRF-Chem model has been developed and applied to study the contribution of different
91 pathways to the sulfate formation in BTH during the summer of 2015. The model
92 configuration and methodology are described in Section 2. Results and discussions are
93 presented in Section 3. The conclusions and summaries are drawn in Section 4.

94

95 **2 Model and methodology**

96 **2.1 WRF-CHEM model and configuration**

97 A specific version of the WRF-Chem model (Grell et al., 2005) developed by Li et al.
98 (2010; 2011a; 2011b; 2012) at the Molina Center for Energy and the Environment is used in
99 the present study. Detailed model description can be found in previous studies (Li et al., 2018;
100 Wu et al., 2017; Feng et al., 2016; Xing et al., 2019). Briefly, the model includes a new
101 flexible gas-phase chemical module and the Community Multi-scale Air Quality (CMAQ)
102 aerosol module developed by the US EPA (Binkowski and Roselle, 2003). The wet
103 deposition uses the method in the CMAQ module and the dry deposition of chemical species
104 is parameterized following Wesely (1989). The photolysis rates are calculated using the Fast
105 Tropospheric Ultraviolet and Visible Radiation Model (FTUV; Li et al., 2005; Tie et al.,
106 2003), with the aerosol and cloud effects on the photochemistry (Li et al., 2011a). The
107 ISORROPIA Version 1.7 is applied to calculate the inorganic components (Nenes et al.,
108 1998). The secondary organic aerosol (SOA) is simulated using a non-traditional module,
109 including the volatility basis-set (VBS) modeling approach and SOA contributions from
110 glyoxal and methylglyoxal. The anthropogenic emission inventory with a horizontal
111 resolution of 6km is developed by Zhang et al. (2009), with the base year of 2013, including
112 industry, transportation, power plant, residential and agriculture sources. The Model of

113 Emissions of Gases and Aerosols from Nature (MEGAN) is used to calculate the biogenic
114 emissions online (Guenther et al., 2006).

115 Traditionally, the brute force method (BFM) is generally used to quantify the formation
116 pathway of particulate matters and chemical compounds in modeling studies (Dunker et al.,
117 1996). The BFM method evaluates the importance of the certain formation pathway through
118 including and excluding the pathway in simulations, but it lacks consideration of interactions
119 of the complicated physical and chemical processes in the atmosphere (Zhang and Ying,
120 2011). The source-oriented method introduces additional chemical species to represent
121 formations from different pathways, providing direct and quantitative determination of
122 contributions of different pathways (Ying and Krishnan, 2010). The coupled source-oriented
123 method air quality models have been widely used to study source apportionment of
124 particulate matters and chemical compounds. Detailed description about the method can be
125 found in previous studies (Ying and Kleeman, 2006; Ying and Krishnan, 2010; Zhang and
126 Ying, 2011). In the present study, four reactive tagged species are introduced to track the
127 sulfate formation pathways.

128 A persistent air pollution episode with high levels of O₃ and PM_{2.5} from 04 to 15 July
129 2015 in BTH is simulated in association with the observation of air pollutants and secondary
130 aerosols. Detailed information about the episode can be found in Wu et al. (2017). Figure 1
131 shows the WRF-Chem model simulation domain and Table 1 presents the model
132 configuration.

133 **2.2 Simulations for the sulfate aerosols**

134 Four sulfate formation pathways are considered in the WRF-Chem model, including (1)
135 the heterogeneous reaction of SO₂ involving aerosol water (hereafter referred to as HR_SO₂),
136 (2) the SO₂ oxidation by OH (hereafter referred to as OH_SO₂), (3) the primary emission, and
137 (4) the SO₂ oxidation by sCI (hereafter referred to as sCI_SO₂). The sulfate formed in the

138 four pathways is tagged and traced in the model to study their contributions to the sulfate
139 formation. It is worth noting that the WRF-Chem model cannot well resolve clouds formed in
140 the planetary boundary layer (PBL), so the aqueous SO₂ oxidation in cloud or fog droplets is
141 not considered in the study, which might cause the sulfate underestimation, and on the other
142 hand might overestimate the contributions of the four pathways to the sulfate concentration.
143 The HR_SO₂ is parameterized as a first-order irreversible uptake of SO₂ by aerosol water,
144 with a reactive uptake coefficient of 0.5×10^{-4} , assuming that alkalinity is sufficient to
145 maintain the high iron-catalyzed reaction rate in BTH (Li et al., 2017). The aerosol
146 hygroscopic growth is directly predicted by ISORROPIA in the model, and the aerosol water
147 surface area is scaled from the calculated wet aerosol surface area using the third-moment of
148 aerosol species.

149 Effects of the sCI chemistry on the sulfate formation depend on κ_{sCI+SO_2} and κ_{sCI+H_2O} ,
150 as well as the sCI precursor concentration. In the study, sCI are assumed to yield from the
151 ozonolysis reaction of five alkenes based on the SAPRC99 mechanism, including ethene
152 (ETHE), terminal olefin (OLE1), internal olefin (OLE2), isoprene (ISOP), and monoterpenes
153 (TERP). Detailed information about the sCI chemistry associated with the sulfate formation
154 can be found in Table 2.

155 CH₂OO (sCI₁) is used to represent sCI produced from the ozonolysis reaction of ETHE
156 and OLE1 and the sCI yield of the two reactions are described in Sarwar et al. (2013).
157 CH₃CHOO (sCI₂) is formed from the ozonolysis reaction of OLE2, and proposed to have two
158 isomers: *syn*-CH₃CHOO and *ant*-CH₃CHOO (Anglada et al., 2011). The reported reaction
159 rate constants of *syn*-CH₃CHOO and *ant*-CH₃CHOO with H₂O are 3.23×10^{-18} and 3.23×10^{-13}
160 cm³ s⁻¹, respectively. We use *syn*-CH₃CHOO (sCI₂) to represent the sCI from the ozonolysis
161 reaction of OLE2 to minimize the removal of sCI by water vapor and maximize sulfate
162 production following Ying et al. (2014). sCI₃ is used to represent sCI from the ozonolysis

163 reaction of isoprene and monoterpenes, and the detailed chemistry of sCI₃
164 (*syn*-CH₃-*anti*-(*cis*-CH=CH₂)CHOO) is described in Sarwar et al. (2013, 2014).

165 In the base case (hereafter referred to as B-case) simulation used to compare with
166 observations in BTH, we use a single κ_{sCI+SO_2} reported by Welz et al. (2012) for reactions
167 of SO₂ with sCI_{1,2,3}. For removal of sCI_{1,2,3} by water vapor, we employ the κ_{sCI+H_2O}
168 suggested by Ying et al. (2014). While not important, the reaction of sCI_{1,2,3} with NO₂ is also
169 implemented in the model, and the rate constant is taken from Welz et al. (2012).

170 **2.3 Observations**

171 Simulations are compared to available meteorological and air pollutants observations to
172 validate the model performance. The meteorological parameters including surface
173 temperature (TSFC), relative humidity (RH), wind speed and direction with a 3-hour interval
174 are obtained from the website <http://www.meteomanz.com>. The hourly measurements of
175 PM_{2.5}, O₃, SO₂, and NO₂ used in this study are downloaded from the website
176 <http://www.aqistudy.cn>. The submicron sulfate, nitrate, ammonium, and organic particulate
177 matters are observed by the Aerodyne Aerosol Chemical Speciation Monitor (ACSM) at the
178 National Center for Nanoscience and Technology (NCNST), Chinese Academy of Sciences,
179 Beijing (116.39°E, 39.99°N). Detailed description about the methods to obtain the primary
180 organic aerosol (POA) and secondary organic aerosol (SOA) mass concentration from the
181 results of ACSM are given in Wu et al. (2017). Figure 1 shows the locations of the ambient
182 air quality monitoring sites and the NCNST observation site.

183 **2.4 Statistical methods for model evaluation**

184 In this study, the mean bias (MB), root mean square error (RMSE) and the index of
185 agreement (IOA) are used to evaluate the model performance:

$$186 \quad MB = \frac{1}{N} \sum_{i=1}^N (P_i - O_i) \quad (1)$$

187
$$RMSE = \left[\frac{1}{N} \sum_{i=1}^N (P_i - O_i)^2 \right]^{\frac{1}{2}} \quad (2)$$

188
$$IOA = 1 - \frac{\sum_{i=1}^N (P_i - O_i)^2}{\sum_{i=1}^N (|P_i - \bar{O}| + |O_i - \bar{O}|)^2} \quad (3)$$

189 Where P_i and O_i are the simulated and observed variables, respectively. N is the total
190 number of the simulations for comparisons, and \bar{O} donates the average of the observation.

191 The IOA ranges from 0 to 1, with 1 showing a perfect agreement of the simulation with the
192 observation.

193

194 **3 Results and discussions**

195 **3.1 Model evaluation**

196 3.1.1 Meteorological parameters simulations in Beijing

197 Considering the key role of meteorological conditions in air pollution simulations (Bei
198 et al., 2012, 2017), Figure 2 shows the temporal profiles of observed and simulated TSFC,
199 RH, wind speed and wind direction from 04 to 15 July 2015 at the weather station in Beijing
200 (Figure 1). The WRF-Chem model generally well replicates the temporal variation of the
201 TSFC during the whole episode compared to observations, with the MB and IOA of 0.7°C
202 and 0.95, respectively. The model considerably overestimates TSFC on July 4 and in the
203 evening of July 13 and 14. The model also performs reasonably well in simulating the RH
204 against observations, with the MB and IOA of -5.3% and 0.84, respectively. The observed
205 high RH exceeding 75% during nighttime is generally well captured, except on July 4 and 14
206 when the TSFC is overestimated. In addition, the model also reasonably well tracks the
207 temporal variations of the wind speed and direction compared to observations, with an IOA
208 of around 0.60. In general, the reasonable simulations of meteorological fields provide a
209 reliable basis for modeling the O₃ and PM_{2.5} pollution episode in the present study.

210 3.1.2 Air pollutant simulations in BTH

211 Figure 3 shows the diurnal profiles of measured and simulated PM_{2.5}, O₃, NO₂, SO₂, and
212 CO mass concentrations averaged over all ambient monitoring stations in BTH during the
213 episode. Apparently, the WRF-Chem model exhibits good performance in simulating the
214 temporal variations of PM_{2.5} and O₃ mass concentrations against observations in BTH, with
215 the IOAs of around 0.90. However, the model fails to capture the observed high PM_{2.5}
216 concentration on July 11 and 12, and frequently overestimates O₃ concentration in the
217 evening, with a MB of 1.2 μg m⁻³. The simulated temporal variation of NO₂ mass
218 concentrations is also generally consistent with observations in BTH, but the model
219 frequently overestimates NO₂ concentrations against observations during nighttime, which
220 might be caused by the low simulated planetary boundary layer (PBL) height or the O₃
221 overestimation. Simulations of the SO₂ mass concentration are not as good as those of other
222 pollutants in BTH during the episode, with an IOA of 0.45. During summertime, SO₂ is
223 principally emitted by the point source, including the power plants and agglomerated
224 industrial zones, so the uncertainties of simulated wind fields substantially affect the SO₂
225 simulations. Additionally, the model overestimation of SO₂ concentrations is also
226 considerable during nighttime, which is perhaps due to the simulated low PBL height. It is
227 worth noting that NH₃ plays an important role in the sulfate formation (Wang et al., 2016;
228 Cheng et al., 2016), so it is imperative to validate NH₃ simulations using measurements.
229 However, due to lack of routine measurements of NH₃ in BTH, the validation of the NH₃
230 simulation is not provided in the study.

231 Figure 4 presents the distributions of simulated and observed near-surface mass
232 concentrations of PM_{2.5}, O₃, NO₂ and SO₂ along with the simulated wind fields averaged
233 from 04 to 15 July 2015. Generally, the simulated wind in BTH is weak during the episode
234 and the easterly wind prevails, which is favorable for the accumulation of air pollutants,
235 particularly along the Taihang and Yanshan Mountains due to the blocking effect. The model

236 generally well reproduces the spatial distribution of $\text{PM}_{2.5}$ concentrations against
237 observations, with the $\text{PM}_{2.5}$ concentration exceeding $35 \mu\text{g m}^{-3}$ in the plain area of BTH
238 (Figure 4a). The average simulated peak O_3 concentrations are more than $200 \mu\text{g m}^{-3}$ during
239 the episode in the plain area of BTH, consistent with the measurement and showing the
240 severe O_3 pollution (Figure 4b). High levels of O_3 indicate a strong atmospheric oxidation
241 capacity (AOC), facilitating the photochemical reactions over BTH (Figure 4b). The
242 simulated high NO_2 and SO_2 concentrations are generally concentrated in cities and their
243 surrounding areas, in agreement with the measurement (Figures 4c and 4d). However, the
244 model considerably overestimates the NO_2 concentrations against the measurement in Beijing,
245 Shijiazhuang and Handan city. In addition, the SO_2 concentrations in BTH are much lower
246 than those during wintertime (Li et al., 2018; Xing et al., 2019), generally less than $30 \mu\text{g m}^{-3}$.
247 Reduced SO_2 concentrations in BTH during summertime are caused by the efficient removal
248 of gas-phase oxidations due to the high AOC, the reduction of residential coal combustion,
249 and the increased PBL height.

250 3.1.3 Aerosol species simulations in Beijing

251 Figure 5 presents the temporal variations of simulated and observed submicron nitrate,
252 ammonium, SOA and POA mass concentrations at NCNST site in Beijing from 04 to 15 July
253 2015. The WRF-Chem model reasonably reproduces the diurnal variation of the nitrate
254 concentration compared to observations, with the MB and IOA of $-0.7 \mu\text{g m}^{-3}$ and 0.81,
255 respectively (Figure 5a). Nitrate formation is sensitive to the air temperature, and its variation
256 is generally negatively correlated with that of the temperature. When the temperature is
257 lowest in the early morning, the nitrate concentration reaches its peaks; when the temperature
258 is up to 30°C in the afternoon, the nitrate concentration is generally less than $1 \mu\text{g m}^{-3}$. The
259 simulated ammonium profile is generally in agreement with observations, with an IOA of
260 0.71, but the model biases are still large. The model underestimation of the ammonium

261 concentration is considerable on July 11 and 12, and the overestimation is also noticeable on
262 July 6 and 7. The model reasonably reproduces the temporal variation of the SOA and POA
263 concentrations compared to the measurement at the NCNST site, with the IOA of around
264 0.60. The observed SOA concentration exhibits rather large fluctuations from 11 to 15 July
265 2015, which are not well tracked by the model. The model fails to capture the observed large
266 fluctuations of POA concentrations. The POA concentration in Beijing is primarily
267 contributed by direct emissions from vehicles, cooking, coal combustion, biomass burning,
268 and trans-boundary transport from outside of Beijing (Wu et al., 2017; Wu et al., 2018), and
269 the uncertainties in various anthropogenic sources and simulated meteorological fields
270 substantially affect the POA simulations (Bei et al., 2017; Bei et al., 2016).

271 In summary, the WRF-CHEM model performs reasonably well in simulating
272 meteorological fields, air pollutants and aerosol species, providing the underlying basis for
273 further evaluation of the sulfate formation pathway.

274 **3.2 Contributions of four pathways to sulfate formation in Beijing and BTH**

275 Figure 6a provides the diurnal profile of simulated and observed submicron sulfate
276 concentrations at NCNST site in Beijing from 04 to 15 July 2015. The model reasonably well
277 tracks temporal variations of the observed sulfate concentration, with the MB and IOA of
278 $-0.9 \mu\text{g m}^{-3}$ and 0.71, respectively. During 11 to 12 July 2015, the model noticeably
279 underestimates the high sulfate concentrations against the measurement. As mentioned in
280 Section 2, the aqueous oxidation of SO_2 in cloud or fog droplets is not considered in the
281 simulation, which might constitute one of the most possible reasons for the underestimation.

282 Figures 6b-e present the contributions of the four pathways to the sulfate formation
283 during the episode at NCNST site in Beijing. On average, the HR_ SO_2 plays the most
284 important role in the sulfate formation, with a contribution of about 32.1% (Figure 6b). Li et
285 al. (2017) have also shown that the HR_ SO_2 is the dominant sulfate source, contributing

286 around 58.4% to sulfate concentrations in Beijing during wintertime due to the very humid
287 conditions and inefficient sulfate formation from gas-phase SO₂ oxidation due to the low
288 AOC. In this study, the average simulated RH is not high in Beijing, less than 50% during the
289 episode, and high O₃ concentrations enhance the AOC to facilitate the gas-phase SO₂
290 oxidation, causing the decreased sulfate contribution of the HR_SO₂. It is worth noting that
291 the HR_SO₂ relies on the assumption that alkalinity is sufficient to maintain the high
292 iron-catalyzed reaction rate (Li et al., 2017). Figure 7 presents the temporal variation of the
293 average simulated aqueous pH in Beijing during the episode. The simulated pH generally
294 fluctuates between 5 and 7, with an average of 6.2, warranting the efficient iron-catalyzed
295 reaction involving aerosol water. High O₃ concentrations substantially increase the sulfate
296 formation efficiency through the SO₂ oxidation by OH and sCI. The OH_SO₂ plays
297 considerable roles in the sulfate formation, with the contribution of 30.8% (Figure 6c). It is
298 worth noting that the primary emission pathway contributes 24.0% of the sulfate
299 concentration at NCNST site.

300 The sCI_SO₂ accounts for about 13.1% of sulfate concentrations at NCNST site, less
301 than the contribution of the other three pathways. Effects of the sCI_SO₂ on the sulfate
302 formation depend on the κ_{sCI+SO_2} . The reported κ_{sCI+SO_2} from previous studies spans
303 orders of magnitude (Welz et al., 2012; Maudlin et al., 2012; Jenkin et al., 1997). In the
304 present study, an upper limit of the κ_{sCI+SO_2} ($3.9 \times 10^{-11} \text{ cm}^3 \text{ s}^{-1}$) is used in the B-case, which
305 is reported by Welz et al. (2012). Furthermore, the reaction of sCI with H₂O is the main loss
306 pathway for sCI in the atmosphere, and the κ_{sCI+H_2O} used in this study represents a lower
307 limit ($1.97 \times 10^{-18} \text{ cm}^3 \text{ s}^{-1}$) (Ying et al., 2014). Therefore, the contribution of the sCI_SO₂ to
308 the sulfate formation might be overestimated in the present study.

309 Figures 8b-e present the simulated temporal variations of the four pathways to the
310 sulfate concentration averaged over the whole BTH from 04 to 15 July 2015. On average, the

311 HR_SO₂ is still the dominant sulfate source, with a contribution of 35.3% (Figure 8b). The
312 OH_SO₂ plays an important role in the sulfate formation, accounting for 33.1% of sulfate
313 mass (Figure 8c). The primary emission pathway and sCI_SO₂ contributes 22.5% and 9.1%
314 of the sulfate concentration, respectively (Figures 8d and 8e).

315 Figure 9 presents the spatial distribution of contributions of the four pathways to the
316 sulfate formation averaged during the episode. The contribution of the HR_SO₂ to the sulfate
317 formation is substantial in BTH, particularly in the plain area with the sulfate contribution
318 exceeding 4.0 μg m⁻³ and being up to 7.0 μg m⁻³ (Figure 9a). Under the condition of high O₃
319 concentrations, the OH_SO₂ oxidation also becomes an important sulfate source, with a
320 sulfate contribution of more than 3.0 μg m⁻³ in the plain area of BTH, which is comparable to
321 the heterogeneous pathway (Figure 9b). Similar to the spatial distribution of SO₂
322 concentrations, the sulfate contribution of the primary emission is mainly concentrated in
323 cities and their downwind areas (Figure 4c). In the plain area of BTH, the sulfate contribution
324 of the primary emission is more than 2.0 μg m⁻³ on average, and exceeds 7 μg m⁻³ in
325 highly-industrialized cities, such as Shijiazhuang, Tangshan and Xingtai. The sulfate
326 contribution of the sCI_SO₂ is not as important as the other three sources, more than 0.8 μg
327 m⁻³ in the plain area of BTH, and the most striking in Beijing, with a contribution exceeding
328 1.2 μg m⁻³ (Figure 9d).

329 3.3 Sensitivity studies

330 Figure 10 shows the diurnal profiles of sCI₁, sCI₂ and sCI₃ concentrations in BTH from
331 04 to 15 July 2015. The average concentration of sCI₁, sCI₂ and sCI₃ is 1.8, 2.0 and 1.9×10⁴
332 molecules cm⁻³, respectively. Novelli et al. (2017) have estimated the concentration of sCI in
333 the lower troposphere based on the observation in a boreal forest in Finland and in rural
334 southern Germany. The results show that the average concentration of sCI is about 5.0×10⁴
335 molecules cm⁻³, with an order of magnitude uncertainty, generally consistent with our study.

336 Dominant sCI peaks frequently occur during nighttime, mainly caused by the low PBL
337 facilitating accumulation of alkenes and sCI and low reaction rates of sCI with other species
338 (Smith et al., 2015; Stone et al., 2014; Taatjes et al., 2017). It is worth noting that sCI are
339 predominantly quenched by reactions with water vapor in the atmosphere.

340 Considering the large variation of the reported κ_{sCI+SO_2} and the importance of water
341 vapor in the sCI removal, sensitivity studies are further conducted to evaluate the sulfate
342 contribution of the sCI_SO₂ in BTH when the different κ_{sCI+SO_2} and κ_{sCI+H_2O} are used in
343 simulations. In the B-case simulation, an upper limit of the κ_{sCI+SO_2} and a lower limit of
344 κ_{sCI+H_2O} are used. The simulated average sulfate concentration is 10.8 $\mu\text{g m}^{-3}$ in BTH,
345 constituting a major component of PM_{2.5}. The HR_SO₂ and OH_SO₂ constitute the two most
346 important sulfate sources, with the sulfate contribution of 35% and 33%, respectively. The
347 primary emission makes up about 23% of the sulfate in BTH, caused by high SO₂ emissions.
348 The sulfate contribution of the sCI_SO₂ is about 1.0 $\mu\text{g m}^{-3}$ or 9.1%, less than that in Beijing
349 with the higher O₃ concentration. Pierce et al. (2013) have used the same κ_{sCI+SO_2} in
350 GEOS-CHEM model as the B-case in the study, revealing that the H₂SO₄ concentration is
351 increased by 4% due to the sCI_SO₂ on global average. The H₂SO₄ enhancement is 10-25%
352 over forested regions in the Northern Hemisphere (up to 100% in July), but is generally
353 negligible elsewhere. The sulfate contribution of the sCI_SO₂ in BTH is close to those over
354 forested regions in Pierce et al. (2013), which is primarily caused by the increasing trend of
355 O₃ and the high precursors emissions of sCI, such as ethene, isoprene and monoterpenes
356 during summertime in the region. Additionally, Boy et al. (2013) have employed the
357 κ_{sCI+SO_2} reported by Mauldin et al. (2012) and Welz et al. (2012) to verify the sulfate
358 contribution of the sCI_SO₂ in European, showing a H₂SO₄ contribution of as much as 33-46%
359 at the ground level. These different sulfate contributions of the sCI_SO₂ are mainly caused by

360 the variation of the reaction constant of sCI with SO₂, NO₂, and H₂O and the sCI precursors
361 concentration, as well as the atmospheric conditions in simulations (Taatjes, 2017).

362 Although the sCI_SO₂ is not an important sulfate source, its contribution might be
363 overestimated. The κ_{sCI+SO_2} used in the B-case is only measured for the smallest sCI,
364 H₂COO, but the larger sCI (such as those produced from typical larger alkenes in the
365 atmosphere) might have a lower reaction rate with SO₂, and produce stable low volatilities
366 species such as sulfur-bearing secondary ozonides (Spracklen et al., 2011; Vereecken et al.,
367 2012). Additionally, Welz et al. (2012) have measured κ_{sCI+SO_2} at low pressure (4 Torr),
368 making it unclear if those rates are appropriate for atmospheric conditions.

369 In the S1-case, the reported κ_{sCI+SO_2} ($6.0 \times 10^{-13} \text{ cm}^3 \text{ s}^{-1}$) by Mauldin et al. (2012) is
370 used, which is deduced from ozonolysis of α -pinene under boundary-layer atmospheric
371 conditions, and the κ_{sCI+H_2O} and κ_{sCI+NO_2} are the same as those in the B-case. The sulfate
372 contribution of the sCI_SO₂ becomes insignificant, around 0.3 $\mu\text{g m}^{-3}$ or less than 3% of the
373 total simulated sulfate concentration on average during the episode in BTH (Figure 11).
374 Compared to the B-case, the sulfate contribution of the sCI_SO₂ is decreased by more than
375 70% in the S1-case. The substantial reduction reveals that further studies are needed to
376 precisely determine the κ_{sCI+SO_2} .

377 One of the largest uncertainties concerning the lifetime of sCI is related to the κ_{sCI+H_2O} ,
378 but few studies have been conducted to directly measure the κ_{sCI+H_2O} . The reported
379 κ_{sCI+H_2O} varies widely, ranging from 2×10^{-19} to $1 \times 10^{-15} \text{ cm}^3 \text{ s}^{-1}$ (Hatakeyama and Akimoto
380 1994), and several studies show that the κ_{sCI+H_2O} needs to be adjusted when the κ_{sCI+SO_2} is
381 adjusted (Li et al., 2013; Calvert et al., 1978; Suto et al., 1985). In order to evaluate the effect
382 of water vapor on the sCI_SO₂, in the S2-case, the κ_{sCI+H_2O} is increased to $2.4 \times 10^{-15} \text{ cm}^3 \text{ s}^{-1}$
383 based on the reported ratio of κ_{sCI+H_2O} to κ_{sCI+SO_2} (6.1×10^{-5}) (Calvert et al., 1978), and the

384 are the same as those in the B3-case. The average sulfate contribution
385 of sCI_SO₂ is decreased to 0.2% or less than 2% of the total simulated
386 sulfate mass due to the competition of water vapor with SO₂ for sCI (Figure 11).
387 The reaction rate constant κ_{sCI+SO_2} is used in the B3-case, the effect of water vapor on the sCI
388 contribution is not substantial. In the S1 and S2-case, there is a dominant peak of
389 sCI_SO₂ on July 10, which might be caused by the reaction rate constants used
390 in the B3-case. We have performed an additional sensitivity study (S3-case), in which the
391 reaction rate constants κ_{sCI+SO_2} ($2 \times 10^{-11} \text{ cm}^3 \text{ s}^{-1}$) and κ_{sCI+H_2O} ($7.4 \times 10^{-12} \text{ cm}^3 \text{ s}^{-1}$) suggested by Stone
392 et al. (2014) and Stone et al. (2015) are used. The results show that the average sulfate
393 contribution of sCI_SO₂ becomes more insignificant, about $0.06 \mu\text{g m}^{-3}$ or less than 0.6%.
394 In addition, there is an obvious peak around July 10 (Figure 11), indicating that the large
395 quantity in sCI_SO₂ contributions of sCI_SO₂ to sulfate mass is due to the different value of
396 κ_{sCI+SO_2} and κ_{sCI+H_2O} used in the sensitivity studies.

397 It is worth noting that the uncertainty in HR_SO₂, as the most important sulfate source,
398 also influences the sulfate contribution of sCI_SO₂. Several factors influence the
399 heterogeneous reactions of SO₂ on aerosol surfaces, including aerosol water surface area,
400 aerosol acidity, organic coating, et al. In the B-case, the predicted average aerosol liquid
401 water and wet surface area are $18.8 \mu\text{g m}^{-3}$ and $2.4 \times 10^{-4} \text{ m}^2 \text{ m}^{-3}$ in the BTH during the
402 episode, and the uptake coefficient of SO₂ by aerosols (γ) is assumed as 0.5×10^{-4} . To
403 investigate the sensitivity of sCI_SO₂ sulfate contributions to uncertainties in HR_SO₂, we
404 perform sensitivity simulations with γ of 0.25×10^{-4} and 1.0×10^{-4} . The sulfate concentration of
405 HR_SO₂ is affected considerably by the variation of γ , with the average change of -18.3%
406 and 25.6% in BTH during the episode when the γ is assumed as 0.25×10^{-4} and 1.0×10^{-4} ,
407 respectively. However, effects of the γ change to sulfate contributions of sCI_SO₂ is not

408 significant, with the change of -4.4% and 3.9% when the γ is assumed as 0.25×10^{-4} and
409 1.0×10^{-4} , respectively.

410 **4 Summaries and Conclusion**

411 In the present study, a persistent air pollution episode with high O₃ and PM_{2.5}
412 concentrations from 04 to 15 July 2015 in BTH is simulated using a source-oriented
413 WRF-Chem model to study the contributions of four pathways to the sulfate formation. The
414 four sulfate formation pathways include the heterogeneous reaction of SO₂ involving aerosol
415 water (HR_SO₂), the SO₂ oxidation by OH (OH_SO₂), the primary emission, and the SO₂
416 oxidation by sCI (sCI_SO₂).

417 The WRF-Chem model reasonably reproduces the temporal variations of the
418 meteorological parameters compared to observations at the weather station in Beijing. The
419 model performs reasonably well in simulating the temporal profiles and spatial distributions
420 of air pollutant mass concentrations against observations at monitoring sites in BTH. In
421 addition, the simulated diurnal variations of submicron nitrate, ammonium, POA, SOA, and
422 sulfate mass concentrations are generally in good agreements with the measurements at
423 NCNST site in Beijing.

424 On average in BTH during the simulation episode, the HR_SO₂ plays the most
425 important role in the sulfate formation, with a sulfate contribution of about 35%. Under
426 conditions with the high O₃ concentration during summertime, the OH_SO₂ also constitutes a
427 major sulfate source comparable to the HR_SO₂, accounting for about 33% of the total
428 simulated sulfate concentration in BTH. Due to high SO₂ emissions, the primary emission
429 contributes about 23% of the sulfate concentration in BTH, mainly concentrated in cities and
430 their downwind regions.

431 When an upper limit of the κ_{sCI+SO_2} ($3.9 \times 10^{-11} \text{ cm}^3 \text{ s}^{-1}$) and a lower limit of κ_{sCI+H_2O}
432 ($1.97 \times 10^{-18} \text{ cm}^3 \text{ s}^{-1}$) are used, the sCI_SO₂ plays an appreciable role in the sulfate formation,

433 with a contribution of around 9%. However, there still exist large uncertainties in
434 contributions of the sCI_SO₂ to the sulfate formation. Sensitivity studies reveal that the
435 sulfate contribution of the sCI_SO₂ is substantially decreased to less than 3%, when the
436 κ_{sCI+SO_2} is decreased to $6.0 \times 10^{-13} \text{ cm}^3 \text{ s}^{-1}$ but the lower limit of κ_{sCI+H_2O} remains.
437 Furthermore, when the κ_{sCI+H_2O} is increased to $2.38 \times 10^{-15} \text{ cm}^3 \text{ s}^{-1}$ based on the reported
438 ratio of κ_{sCI+H_2O} to κ_{sCI+SO_2} ($6.1 \times 10^{-5} \text{ cm}^3 \text{ s}^{-1}$) but the upper limit of the κ_{sCI+SO_2} remains,
439 the sulfate contribution of the reaction becomes insignificant, less than 2%. Future studies
440 still need to be conducted to measure the κ_{sCI+SO_2} and κ_{sCI+H_2O} under the atmospheric
441 condition to better evaluate effects of the sCI chemistry on the sulfate formation.
442 Additionally, as a potentially important atmospheric oxidant, sCI may enhance ozone
443 formation and ultimately the OH formation. The indirect effects of sCI on the sulfate
444 formation by promoting the OH_SO₂ pathway should also be investigated further.

445

446

447 *Author contribution.* Guohui Li, as the contact author, provided the ideas and financial
448 support, verified the conclusions, and revised the paper. Lang Liu conducted a research,
449 designed the experiments, carried the methodology out, performed the simulation, processed
450 the data, prepared the data visualization, and prepared the manuscript with contributions from
451 all authors. Naifang Bei, Jiarui Wu and Xia Li provided the treatment of meteorological data,
452 analyzed the study data, validated the model performance, and reviewed the manuscript.
453 Suixin Liu, Qingchuan Yang, Tian Feng, and Jiamao Zhou provided the observation data
454 used in the study, synthesized the observation, and reviewed the paper. Xuexi Tie and Junji
455 Cao provided critical reviews pre-publication stage.

456

457

458 *Acknowledgements.* This work is financially supported by the National Key R&D Plan
459 (Quantitative Relationship and Regulation Principle between Regional Oxidation Capacity of
460 Atmospheric and Air Quality (2017YFC0210000)) and National Research Program for Key
461 Issues in Air Pollution Control (DQGG0105).
462

463 **References**

- 464 Anglada, J. M., González, J., Torrent-Sucarrat, M.: Effects of the substituents on the
465 reactivity of carbonyl oxides. A theoretical study on the reaction of substituted carbonyl
466 oxides with water, *Phys. Chem. Chem. Phys.*, 13(28), 13034–13045,
467 <https://doi.org/10.1039/C1CP20872A>, 2011.
- 468 Bei, N., Li, G., Huang, R.-J., Cao, J., Meng, N., Feng, T., Liu, S., Zhang, T., Zhang, Q., and
469 Molina, L. T.: Typical synoptic situations and their impacts on the wintertime air
470 pollution in the Guanzhong basin, China, *Atmos. Chem. Phys.*, 16, 7373–7387,
471 <https://doi.org/10.5194/acp-16-7373-2016>, 2016.
- 472 Bei, N., Li, G., and Molina, L. T.: Uncertainties in SOA simulations due to meteorological
473 uncertainties in Mexico City during MILAGRO-2006 field campaign, *Atmos. Chem.*
474 *Phys.*, 12, 11295–11308, <https://doi.org/10.5194/acp-12-11295-2012>, 2012.
- 475 Bei, N., Wu, J., Elser, M., Feng, T., Cao, J., El-Haddad, I., Li, X., Huang, R., Li, Z., Long, X.,
476 Xing, L., Zhao, S., Tie, X., Prévôt, A. S. H., and Li, G.: Impacts of meteorological
477 uncertainties on the haze formation in Beijing-Tianjin-Hebei (BTH) during wintertime:
478 a case study, *Atmos. Chem. Phys.*, 17, 14579–14591,
479 <https://doi.org/10.5194/acp-17-14579-2017>, 2017.
- 480 Binkowski, F. S. and Roselle, S. J.: Models-3 Community Multiscale Air Quality (CMAQ)
481 model aerosol component 1. Model description, *J. Geophys. Res.-Atmos.*, 108, 335–346,
482 <https://doi.org/10.1029/2001JD001409>, 2003.
- 483 Boy, M., Mogensen, D., Smolander, S., Zhou, L., Nieminen, T., Paasonen, P., Plass-Dülmer,
484 C., Sipilä, M., Petäjä, T., Mauldin, L., Berresheim, H., and Kulmala, M.: Oxidation of
485 SO₂ by stabilized Criegee intermediate (sCI) radicals as a crucial source for atmospheric
486 sulfuric acid concentrations, *Atmos. Chem. Phys.*, 13, 3865–3879,
487 <https://doi.org/10.5194/acp-13-3865-2013>, 2013.
- 488 Calvert, J. G., Su, F., Bottenheim, J. W., and Strausz, O. P.: Mechanism of the homogeneous
489 oxidation of sulfur dioxide in the troposphere, *Atmos. Environ.*, 12, 197–226,
490 [https://doi.org/10.1016/0004-6981\(78\)90201-9](https://doi.org/10.1016/0004-6981(78)90201-9), 1978.
- 491 Chen, F. and Dudhia, J.: Coupling an advanced land surface-hydrology model with the Penn
492 State-NCAR MM5 modeling system. Part I: Model implementation and sensitivity, *Mon.*
493 *Weather Rev.*, 129, 569–585,
494 [https://doi.org/10.1175/1520-0493\(2001\)129<0569:CAALSH>2.0.CO;2](https://doi.org/10.1175/1520-0493(2001)129<0569:CAALSH>2.0.CO;2), 2001.
- 495 Cheng, Y., Zheng, G., Wei, C., Mu, H., Zheng, B., Wang, Z., Gao, M., Zhang, Q., He, K.,
496 Carmichael, G., Pöschl, U., and Su, H.: Reactive nitrogen chemistry in aerosol water as
497 a source of sulfate during haze events in China, *Sci. Adv.*, 2(12), e1601530,
498 <https://doi.org/10.1126/sciadv.1601530>, 2016.
- 499 Chou, M. D. and Suarez, M. J.: A solar radiation parameterization for atmospheric studies,
500 edited by: Suarez, M. J., No. NASA/TM-1999-10460, NASA Technique Report, 1999.
- 501 Chou, M. D., Suarez, M. J., Liang, X. Z., Yan, M. H., and Cote, C.: A Thermal Infrared
502 Radiation Parameterization for Atmospheric Studies, edited by: Suarez, M. J., No.
503 NASA/TM-2001-104606, NASA Technique Report, 2001.

504 Cox, R. A., and Penkett, S. A.: Oxidation of atmospheric SO₂ by products of the
505 Ozone-Olefin reaction, *Nature*, 230, 321–322, <https://doi.org/10.1038/230321a0>, 1971.

506 Dunker, A. M., Morris, R. E., Pollack, A. K., Schleyer, C. H., and Yarwood, G.:
507 Photochemical modeling of the impact of fuels and vehicles on urban ozone using auto
508 oil program data, *Environ. Sci. Technol.*, 30, 787–801,
509 <https://doi.org/10.1021/es950175m>, 1996.

510 Feng, T., Li, G., Cao, J., Bei, N., Shen, Z., Zhou, W., Liu, S., Zhang, T., Wang, Y., Huang,
511 R.-J., Tie, X., and Molina, L. T.: Simulations of organic aerosol concentrations during
512 springtime in the Guanzhong Basin, China, *Atmos. Chem. Phys.*, 16, 10045–10061,
513 <https://doi.org/10.5194/acp-16-10045-2016>, 2016.

514 Gao, M., Carmichael, G. R., Wang, Y., Saide, P. E., Yu, M., Xin, J., Liu, Z., and Wang, Z.:
515 Modeling study of the 2010 regional haze event in the North China Plain, *Atmos. Chem.*
516 *Phys.*, 16, 1673–1691, <https://doi.org/10.5194/acp-16-1673-2016>, 2016.

517 Grell, G. A., Peckham, S. E., Schmitz, R., McKeen, S. A., Frost, G., Skamarock, W. C., and
518 Eder, B.: Fully coupled “online” chemistry within the WRF model, *Atmos. Environ.*, 39,
519 6957–6975, <https://doi.org/10.1016/j.atmosenv.2005.04.027>, 2005.

520 Guenther, A., Karl, T., Harley, P., Wiedinmyer, C., Palmer, P. I., and Geron, C.: Estimates of
521 global terrestrial isoprene emissions using MEGAN (Model of Emissions of Gases and
522 Aerosols from Nature), *Atmos. Chem. Phys.*, 6, 3181–3210,
523 <https://doi.org/10.5194/acp-6-3181-2006>, 2006.

524 Guo, S., Hu, M., Zamora, M. L., Peng, J., Shang, D., Zheng, J., Du, Z., Wu, Z., Shao, M., and
525 Zeng, L.: Elucidating severe urban haze formation in China, *P. Natl. Acad. Sci. USA*,
526 111, 17373–17378, <https://doi.org/10.1073/pnas.1419604111>, 2014.

527 Hatakeyama, S. and Akimoto, H.: Reactions of Criegee Intermediates in the gas phase, *Res.*
528 *Chem. Intermed.*, 20, 503–524, <https://doi.org/10.1163/156856794X00432>, 1994.

529 Hong, S. Y. and Lim, J. O. J.: The WRF Single-Moment 6-Class Microphysics Scheme
530 (WSM6), *Asia-Pacif. J. Atmos. Sci.*, 42, 129–151, 2006.

531 Horowitz, L. W., Walters, S., Mauzerall, D. L., Emmons, L. K., Rasch, P. J., Granier, C., Tie,
532 X., Lamarque, J. F., Schultz, M. G., Tyndall, G. S., Orlando, J. J., and Brasseur, G. P.: A
533 global simulation of tropospheric ozone and related tracers: Description and evaluation
534 of MOZART, version 2, *J. Geophys. Res.-Atmos.*, 108, 4784,
535 <https://doi.org/10.1029/2002JD002853>, 2003.

536 Janjić, Z. I.: Nonsingular Implementation of the Mellor-Yamada Level 2.5 Scheme in the
537 NCEP Meso Model, NCEP Office Note 437, 2002.

538 Jenkin, M. E., Saunders, S. M., and Pilling, M. J.: The tropospheric degradation of volatile
539 organic compounds: a protocol for mechanism development, *Atmos. Environ.*, 31, 81–
540 104, [https://doi.org/10.1016/S1352-2310\(96\)00105-7](https://doi.org/10.1016/S1352-2310(96)00105-7), 1997.

541 Li, G., Bei, N., Cao, J., Huang, R., Wu, J., Feng, T., Wang, Y., Liu, S., Zhang, Q., Tie, X.,
542 and Molina, L. T.: A possible pathway for rapid growth of sulfate during haze days in
543 China, *Atmos. Chem. Phys.*, 17, 3301–3316, <https://doi.org/10.5194/acp-17-3301-2017>,
544 2017.

- 545 Li, G., Bei, N., Tie, X., and Molina, L. T.: Aerosol effects on the photochemistry in Mexico
546 City during MCMA-2006/MILAGRO campaign, *Atmos. Chem. Phys.*, 11, 5169–5182,
547 <https://doi.org/10.5194/acp-11-5169-2011>, 2011a.
- 548 Li, G., Lei, W., Bei, N., and Molina, L. T.: Contribution of garbage burning to chloride and
549 PM_{2.5} in Mexico City, *Atmos. Chem. Phys.* 12, 8751–8761,
550 <https://doi.org/10.5194/acp-12-8751-2012>, 2012.
- 551 Li, G., Lei, W., Zavala, M., Volkamer, R., Dusanter, S., Stevens, P., and Molina, L. T.:
552 Impacts of HONO sources on the photochemistry in Mexico City during the
553 MCMA-2006/MILAGO Campaign, *Atmos. Chem. Phys.*, 10, 6551–6567,
554 <https://doi.org/10.5194/acp-10-6551-2010>, 2010.
- 555 Li, G., Zavala, M., Lei, W., Tsimpidi, A. P., Karydis, V. A., Pandis, S. N., Canagaratna, M.
556 R., and Molina, L. T.: Simulations of organic aerosol concentrations in Mexico City
557 using the WRF-CHEM model during the MCMA-2006/MILAGRO campaign, *Atmos.*
558 *Chem. Phys.*, 11, 3789–3809, <https://doi.org/10.5194/acp-11-3789-2011>, 2011b.
- 559 Li, G., Zhang, R., Fan, J., and Tie, X.: Impacts of black carbon aerosol on photolysis and
560 ozone, *J. Geophys. Res.-Atmos.*, 110, D23206, <https://doi.org/10.1029/2005JD005898>,
561 2005.
- 562 Li, J., Ying, Q., Yi, B., and Yang, P.: Role of stabilized Criegee Intermediates in the
563 formation of atmospheric sulfate in eastern United States, *Atmos. Environ.*, 79, 442–447,
564 <http://dx.doi.org/10.1016/j.atmosenv.2013.06.048>, 2013.
- 565 Li, X., Wu, J., Elser, M., Feng, T., Cao, J., El-Haddad, I., Huang, R., Tie, X., Prévôt, A. S. H.,
566 and Li, G.: Contributions of residential coal combustion to the air quality in Beijing–
567 Tianjin–Hebei (BTH), China: a case study, *Atmos. Chem. Phys.*, 18, 10675–10691,
568 <https://doi.org/10.5194/acp-18-10675-2018>, 2018.
- 569 Mauldin, R. L., Berndt, T., Sipilä, M., Paasonen, P., Petäjä, T., Kim, S., Kurtén, T.,
570 Stratmann, F., Kerminen, V. M., and Kulmala, M.: A new atmospherically relevant
571 oxidant of sulphur dioxide, *Nature*, 488, 193–196, <https://doi.org/10.1038/nature11278>,
572 2012.
- 573 Nenes, A., Pandis, S. N., and Pilinis, C.: ISORROPIA: A new thermodynamic equilibrium
574 model for multiphase multicomponent inorganic aerosols, *Aquat. Geochem.*, 4, 123–152,
575 <https://doi.org/10.1023/a:1009604003981>, 1998.
- 576 Novelli, A., Hens, K., Tatum Ernest, C., Martinez, M., Nölscher, A. C., Sinha, V., Paasonen,
577 P., Petäjä, T., Sipilä, M., Elste, T., Plass-Dülmer, C., Phillips, G. J., Kubistin, D.,
578 Williams, J., Vereecken, L., Lelieveld, J., and Harder, H.: Estimating the atmospheric
579 concentration of Criegee intermediates and their possible interference in a FAGE-LIF
580 instrument, *Atmos. Chem. Phys.*, 17, 7807–7826,
581 <https://doi.org/10.5194/acp-17-7807-2017>, 2017.
- 582 Percival, C. J., Welz, O., Eskola, A. J., Savee, J. D., Osborn, D. L., Topping, D. O., Lowe, D.,
583 Utembe, S. R., Cooke, M. C., Taatjes, C. A., and Shallcross, D. E.: Regional and global
584 impacts of Criegee intermediates on atmospheric sulphuric acid concentrations and first
585 steps of aerosol formation, *Faraday discussions*, 165, 45–73,
586 <https://doi.org/10.1039/C3FD00048F>, 2013.
- 587 Pierce, J. R., Evans, M. J., Scott, C. E., D'Andrea, S. D., Farmer, D. K., Swietlicki, E., and
588 Spracklen, D. V.: Weak global sensitivity of cloud condensation nuclei and the aerosol

- 589 indirect effect to Criegee + SO₂ chemistry, *Atmos. Chem. Phys.*, 13, 3163–3176,
590 <https://doi.org/10.5194/acp-13-3163-2013>, 2013.
- 591 Sarwar, G., Fahey, K., Kwok, R., Gilliam, R. C., Roselle, S. J., Mathur, R., Xue, J., Yu, J.,
592 and Carter, W. P.: Potential impacts of two SO₂ oxidation pathways on regional sulfate
593 concentrations: Aqueous-phase oxidation by NO₂ and gas-phase oxidation by Stabilized
594 Criegee Intermediates, *Atmos. Environ.*, 68, 186–197,
595 <https://doi.org/10.1016/j.atmosenv.2012.11.036>, 2013.
- 596 Sarwar, G., Simon, H., Fahey, K., Mathur, R., Goliff, W. S., and Stockwell, W. R.: Impact of
597 sulfur dioxide oxidation by Stabilized Criegee Intermediate on sulfate, *Atmos. Environ.*,
598 85, 204–214, <https://doi.org/10.1016/j.atmosenv.2013.12.013>, 2014.
- 599 Seinfeld, J. H. and Pandis, S. N.: *Atmospheric Chemistry and Physics: From Air Pollution to*
600 *Climate Change*, 2nd Edn., John Wiley & Sons Inc., New York, 2006.
- 601 Smith, M., Chang, C-H., Chao, W., Lin, L-C., Takahashi, K., Boering, K., and Lin, J. J-M:
602 Strong negative temperature dependence of the simplest Criegee Intermediate CH₂OO
603 reaction with water dimer, *J. Phys. Chem. Lett.*, 6(14), 2708–2713,
604 <https://doi.org/10.1021/acs.jpcclett.5b01109>, 2015.
- 605 Spracklen, D. V., Jimenez, J. L., Carslaw, K. S., Worsnop, D. R., Evans, M. J., Mann, G. W.,
606 Zhang, Q., Canagaratna, M. R., Allan, J., Coe, H., McFiggans, G., Rap, A., and Forster,
607 P.: Aerosol mass spectrometer constraint on the global secondary organic aerosol budget,
608 *Atmos. Chem. Phys.*, 11, 12109–12136, <https://doi.org/10.5194/acp-11-12109-2011>,
609 2011.
- 610 Stone, D., Blitz, M., Daubney, L., Howes, N., and Seakins, P.: Kinetics of CH₂OO reactions
611 with SO₂, NO₂, NO, H₂O and CH₃CHO as a function of pressure, *Phys. Chem. Chem.*
612 *Phys.*, 16, 1139–1149, <https://doi.org/10.1039/c3cp54391a>, 2014.
- 613 Sun, Y. L., Wang, Z. F., Du, W., Zhang, Q., Wang, Q. Q., Fu, P. Q., Pan, X. L., Li, J., Jayne,
614 J., and Worsnop, D. R.: Long-term real-time measurements of aerosol particle
615 composition in Beijing, China: seasonal variations, meteorological effects, and source
616 analysis, *Atmos. Chem. Phys.*, 15, 10149–10165,
617 <https://doi.org/10.5194/acp-15-10149-2015>, 2015.
- 618 Suto, M., Manzanares, E. R., and Lee, L. C.: Detection of sulfuric-acid aerosols by ultraviolet
619 scattering, *Environ. Sci. Tech.*, 19, 815–820, <https://doi.org/10.1021/es00139a008>,
620 1985.
- 621 Taatjes, C. A.: Criegee intermediates: What direct production and detection can teach us
622 about reactions of carbonyl oxides, *Annu. Rev. Phys. Chem.* 2017. 68:183–207,
623 <https://doi.org/10.1146/annurev-physchem-052516-050739>, 2017.
- 624 Tao, J., Zhang, L., Cao, J., and Zhang, R.: A review of current knowledge concerning PM_{2.5}
625 chemical composition, aerosol optical properties and their relationships across China,
626 *Atmos. Chem. Phys.*, 17, 9485–9518, <https://doi.org/10.5194/acp-17-9485-2017>, 2017.
- 627 Tie, X., Madronich, S., Walters, S., Zhang, R., Rasch, P., and Collins, W.: Effect of clouds on
628 photolysis and oxidants in the troposphere, *J. Geophys. Res.-Atmos.*, 108, 4642,
629 <https://doi.org/10.1029/2003JD003659>, 2003.

- 630 Vereecken, L., Harder, H., and Novelli, A.: The reaction of Criegee intermediates with NO,
631 RO₂, and SO₂, and their fate in the atmosphere, *Phys. Chem. Chem. Phys.*, 14, 14682–
632 14695, <https://doi.org/10.1039/c2cp42300f>, 2012.
- 633 Wang, S., and Hao, J.: Air quality management in China: Issues, challenges, and options, *J.*
634 *Environ. Sci.*, 24, 2–13, [https://doi.org/10.1016/S1001-0742\(11\)60724-9](https://doi.org/10.1016/S1001-0742(11)60724-9), 2012.
- 635 Wang, G., Zhang, R., Gomez, M. E., Yang, L., Levy Zamora, M., Hu, M., Lin, Y., Peng, J.,
636 Guo, S., Meng, J., Li, J., Cheng, C., Hu, T., Ren, Y., Wang, Y., Gao, J., Cao, J., An, Z.,
637 Zhou, W., Li, G., Wang, J., Tian, P., Marrero-Ortiz, W., Secret, J., Du, Z., Zheng, J.,
638 Shang, D., Zeng, L., Shao, M., Wang, W., Huang, Y., Wang, Y., Zhu, Y., Li, Y., Hu, J.,
639 Pan, B., Cai, L., Cheng, Y., Ji, Y., Zhang, F., Rosenfeld, D., Liss, P. S., Duce, R. A.,
640 Kolb, C. E., and Molina, M. J.: Persistent sulfate formation from London Fog to Chinese
641 haze, *P. Natl. Acad. Sci. USA*, 113(48), 13630–13635,
642 <https://doi.org/10.1073/pnas.1616540113>, 2016.
- 643 Welz, O., Savee, J. D., Osborn, D. L., Vasu, S. S., Percival, C. J., Shallcross, D. E., and
644 Taatjes, C.A: Direct kinetic measurements of Criegee Intermediate (CH₂OO) formed by
645 reaction of CH₂I with O₂, *Science*, 335, 204–207,
646 <https://doi.org/10.1126/science.1213229>, 2012.
- 647 Wesely, M. L.: Parameterization of surface resistances to gaseous dry deposition in
648 regional-scale numerical models, *Atmos. Environ.*, 23, 1293–1304,
649 [https://doi.org/10.1016/0004-6981\(89\)90153-4](https://doi.org/10.1016/0004-6981(89)90153-4), 1989.
- 650 Wu, J., Li, G., Cao, J., Bei, N., Wang, Y., Feng, T., Huang, R., Liu, S., Zhang, Q., and Tie, X.:
651 Contributions of trans-boundary transport to summertime air quality in Beijing, China,
652 *Atmos. Chem. Phys.*, 17, 2035–2051, <https://doi.org/10.5194/acp-17-2035-2017>, 2017.
- 653 Wu, J., Bei, N., Li, X., Cao, J., Feng, T., Wang, Y., Tie, X., and Li, G.: Widespread air
654 pollutants of the North China Plain during the Asian summer monsoon season: a case
655 study, *Atmos. Chem. Phys.*, 18, 8491–8504, <https://doi.org/10.5194/acp-18-8491-2018>,
656 2018.
- 657 Xing, L., Wu, J., Elser, M., Tong, S., Liu, S., Li, X., Liu, L., Cao, J., Zhou, J., El-Haddad, I.,
658 Huang, R., Ge, M., Tie, X., Prévôt, A. S. H., and Li, G.: Wintertime secondary organic
659 aerosol formation in Beijing–Tianjin–Hebei (BTH): contributions of HONO sources and
660 heterogeneous reactions, *Atmos. Chem. Phys.*, 19, 2343–2359,
661 <https://doi.org/10.5194/acp-19-2343-2019>, 2019.
- 662 Ying Q., Cureno, I. V., Chen, G., Ali, S., Zhang, H., Malloy, M., Bravo, H. A., and Sosa, R.:
663 Impacts of stabilized Criegee Intermediates, surface uptake processes and higher
664 aromatic secondary organic aerosol yields on predicted PM_{2.5} concentrations in the
665 Mexico City Metropolitan Zone, *Atmos. Environ.*, 94, 438–447,
666 <http://dx.doi.org/10.1016/j.atmosenv.2014.05.056>, 2014.
- 667 Ying, Q. and Kleeman, M. J.: Source contributions to the regional distribution of secondary
668 particulate matter in California, *Atmos. Environ.*, 40: 736–752,
669 <https://doi.org/10.1016/j.atmosenv.2005.10.007>, 2006.
- 670 Ying, Q. and Krishnan, A.: Source contribution of volatile organic compounds to ozone
671 formation in southeast Texas, *J. Geophys. Res.-Atmos.*, 115, D17306,
672 <https://doi.org/10.1029/2010JD013931>, 2010.

- 673 Zhang, H. and Ying, Q.: Secondary organic aerosol formation and source apportionment in
674 Southeast Texas, *Atmos. Environ.*, 45: 3217–3227,
675 <https://doi.org/10.1016/j.atmosenv.2011.03.046>, 2011.
- 676 Zhang, Q., Streets, D. G., Carmichael, G. R., He, K., Huo, H., Kannari, A., Klimont, Z., Park,
677 I. S., Reddy, S., Fu, J., Chen, D., Duan, L., Lei, Y., Wang, L., and Yao, Z.: Asian
678 emissions in 2006 for the NASA INTEX-B mission, *Atmos. Chem. Phys.*, 9, 5131–5153,
679 <https://doi.org/10.5194/acp-9-5131-2009>, 2009.
- 680 Zhang, X. Y., Wang, Y. Q., Niu, T., Zhang, X. C., Gong, S. L., Zhang, Y. M., and Sun, J. Y.:
681 Atmospheric aerosol compositions in China: spatial/temporal variability, chemical
682 signature, regional haze distribution and comparisons with global aerosols, *Atmos.*
683 *Chem. Phys.*, 12, 779–799, <https://doi.org/10.5194/acp-12-779-2012>, 2012.
- 684 Zhao, P. S., Dong, F., He, D., Zhao, X. J., Zhang, X. L., Zhang, W. Z., Yao, Q., and Liu, H.
685 Y.: Characteristics of concentrations and chemical compositions for PM_{2.5} in the region
686 of Beijing, Tianjin, and Hebei, China, *Atmos. Chem. Phys.*, 13, 4631–4644,
687 <https://doi.org/10.5194/acp-13-4631-2013>, 2013.
- 688
- 689

690 Table 1 WRF-CHEM model configurations.

691

Regions	Beijing-Tianjin-Hebei (BTH)
Simulation period	July 4 to 15, 2015
Domain size	300 × 300
Domain center	38.0°N, 116.0°E
Horizontal resolution	6km × 6km
Vertical resolution	35 vertical levels with a stretched vertical grid with spacing ranging from 30m near the surface, to 500m at 2.5km and 1km above 14km
Microphysics scheme	WSM 6-class graupel scheme (Hong and Lim, 2006)
Boundary layer scheme	MYJ TKE scheme (Janjić, 2002)
Surface layer scheme	MYJ surface scheme (Janjić, 2002)
Land-surface scheme	Unified Noah land-surface model (Chen and Dudhia, 2001)
Long-wave radiation scheme	Goddard longwave scheme (Chou and Suarez, 2001)
Short-wave radiation scheme	Goddard shortwave scheme (Chou and Suarez, 1999)
Meteorological boundary and initial conditions	ERA-Interim 0.125°×0.125° reanalysis data (http://apps.ecmwf.int/datasets)
Chemical initial and boundary conditions	MOZART 6-hour output (Horowitz et al., 2003) (https://www.acom.ucar.edu/wrf-chem/mozart.shtml)
Anthropogenic emission inventory	SAPRC-99 chemical mechanism emissions (Zhang et al., 2009)
Biogenic emission inventory	MEGAN model developed by Guenther et al. (2006)
Four-dimension data assimilation	NCEP ADP Global Air Observational Weather Data (https://rda.ucar.edu/datasets)
Model spin-up time	24 hours

692

693

694

695

696

697 Table 2 Reactions and rate constants related to the sCI chemistry
 698

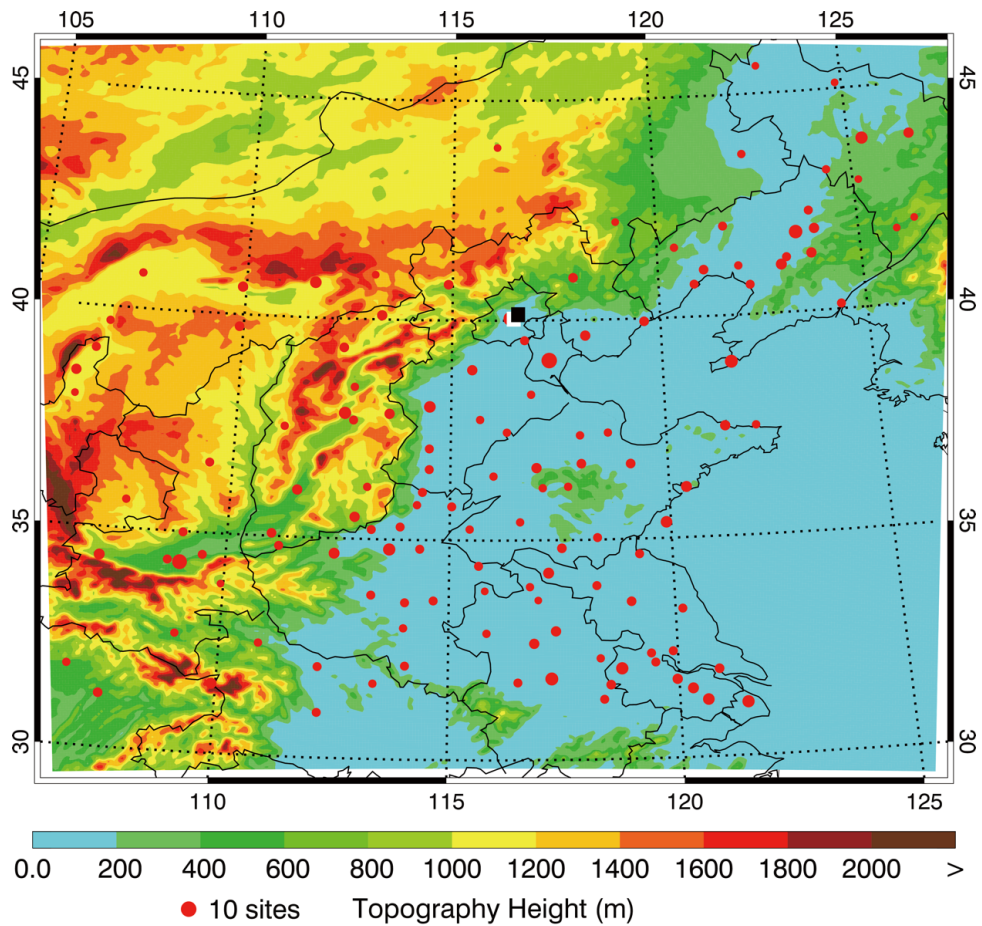
Reaction	Rate constant (cm ³ s ⁻¹)	References
ETHE + O ₃ → ... + 0.37×sCI ₁	9.14×10 ⁻¹⁵	Sarwar et al. (2013)
OLE1 + O ₃ → ... + 0.319×sCI ₁	2.62×10 ⁻¹⁵	Sarwar et al. (2013)
OLE2 + O ₃ → ... + 0.319×sCI ₂	5.02×10 ⁻¹⁶	Sarwar et al. (2013)
ISOP + O ₃ → ... + 0.22×sCI ₃	7.88×10 ⁻¹⁵	Sarwar et al. (2013)
TERP + O ₃ → ... + 0.21×sCI ₃	1.08×10 ⁻¹⁵	Sarwar et al. (2013)
sCI _{1,2,3} + SO ₂ → SULF	3.9×10 ⁻¹¹	Welz et al. (2012)
sCI _{1,2,3} + NO ₂ → NO ₃	7.0×10 ⁻¹²	Welz et al. (2012)
sCI _{1,2,3} + H ₂ O →	1.97×10 ⁻¹⁸	Ying et al. (2014)

699 Note: SULF represents sulfuric acid.

700
 701
 702
 703
 704

Figure Captions

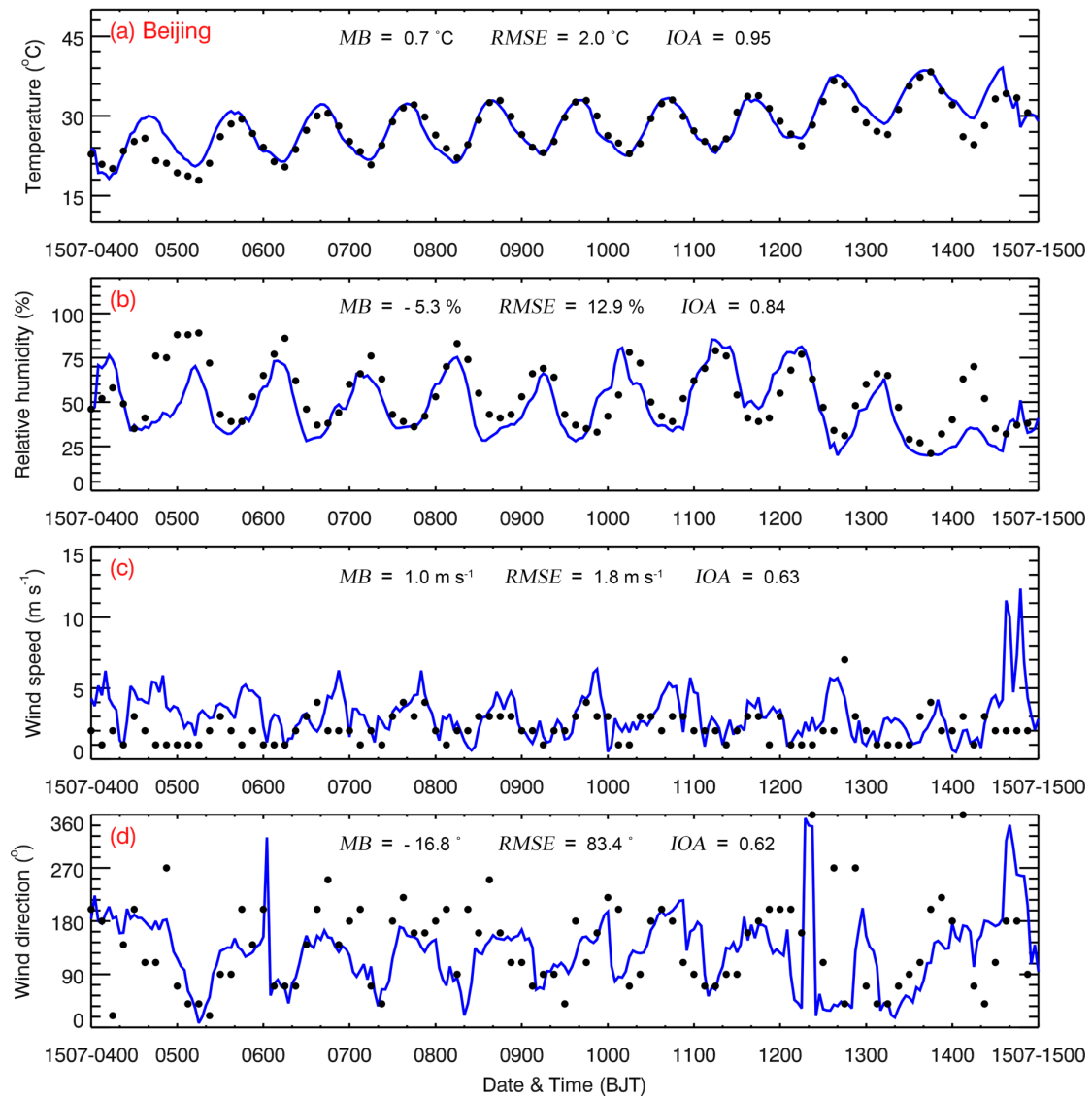
- 705
706
- 707 Figure 1 WRF-Chem simulation domain with topography height. The red filled circles show
708 the locations of the cities with ambient air quality monitoring sites, and the size of the
709 circles represents the number of sites in each city. The white and black filled rectangle
710 denotes the weather station and NCNST observation site in Beijing.
- 711 Figure 2 Temporal variations of the simulated (blue line) and observed (black dots)
712 near-surface (a) temperature, (b) relative humidity, (c) wind speed, and (d) wind
713 direction at the weather station in Beijing from 04 to 15 July 2015.
- 714 Figure 3 Comparison of observed (black dots) and simulated (blue line) diurnal profiles of
715 near surface hourly (a) PM_{2.5}, (b) O₃, (c) NO₂, and (d) SO₂ averaged over all ambient
716 monitoring stations in BTH from 04 to 15 July 2015.
- 717 Figure 4 Spatial distributions of average (a) PM_{2.5}, (b) peak O₃, (c) NO₂, and (d) SO₂ mass
718 concentrations from 04 to 15 July 2015. Colored dots, colored contour, and black
719 arrows are observations and simulations of air pollutants, and simulated surface winds,
720 respectively.
- 721 Figure 5 Comparison of observed (black dots) and simulated (blue line) diurnal profiles of
722 hourly submicron (a) nitrate, (b) ammonium, (c) SOA, and (d) POA mass
723 concentrations at NCNST site in Beijing from 04 to 15 July 2015.
- 724 Figure 6 (a) Comparison of observed (black dots) and simulated (blue line) diurnal profiles of
725 hourly submicron sulfate mass concentration, and temporal variation of simulated
726 sulfate contribution of the (b) HR_SO₂, (c) OH_SO₂, (d) primary emission, and (e)
727 sCI_SO₂ to the sulfate concentration at NCNST site in Beijing from 04 to 15 July
728 2015.
- 729 Figure 7 Temporal variation of the average simulated pH in Beijing from 04 to 15 July 2015.
- 730 **Figure 8 (a) Simulated diurnal profiles of total sulfate mass concentration, and contributions**
731 **of the (b) HR_SO₂, (c) OH_SO₂, (d) primary emission, and (e) sCI_SO₂ to the sulfate**
732 **concentration averaged over BTH from 04 to 15 July 2015.**
- 733 **Figure 9** Spatial distributions of average sulfate contributions of the (a) HR_SO₂, (b)
734 OH_SO₂, (c) primary emission, and (d) sCI_SO₂ in BTH from 04 to 15 July 2015.
- 735 **Figure 10** Temporal variations of the simulated concentration of different sCI (Blue line: sCI₁;
736 Green line: sCI₂; Red line: sCI₃) in BTH from 04 to 15 July 2015.
- 737 **Figure 11** Temporal variations of the simulated average sulfate concentration contributed by
738 the sCI_SO₂ (Blue line: B-case; Red line: S1-case; Green line: S2-case; Black line:
739 S3-case) in BTH from 04 to 15 July 2015.
- 740
741
742
743
744



745
746

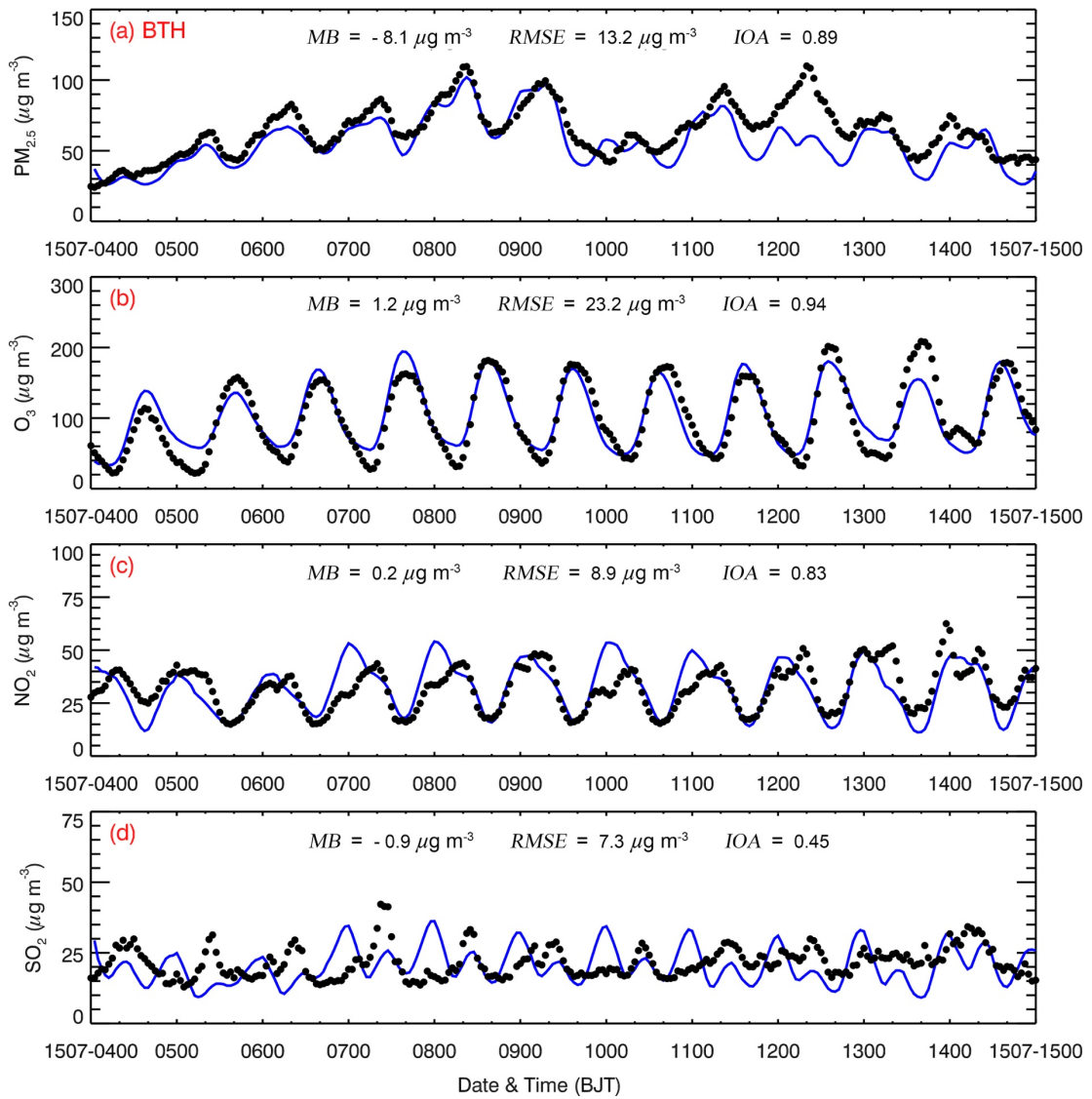
747 Figure 1 WRF-Chem simulation domain with topography height. The red filled circles show
748 the locations of the cities with ambient air quality monitoring sites, and the size of the circles
749 represents the number of sites in each city. The white and black filled rectangle denotes the
750 weather station and NCNST observation site in Beijing.

751
752
753
754
755



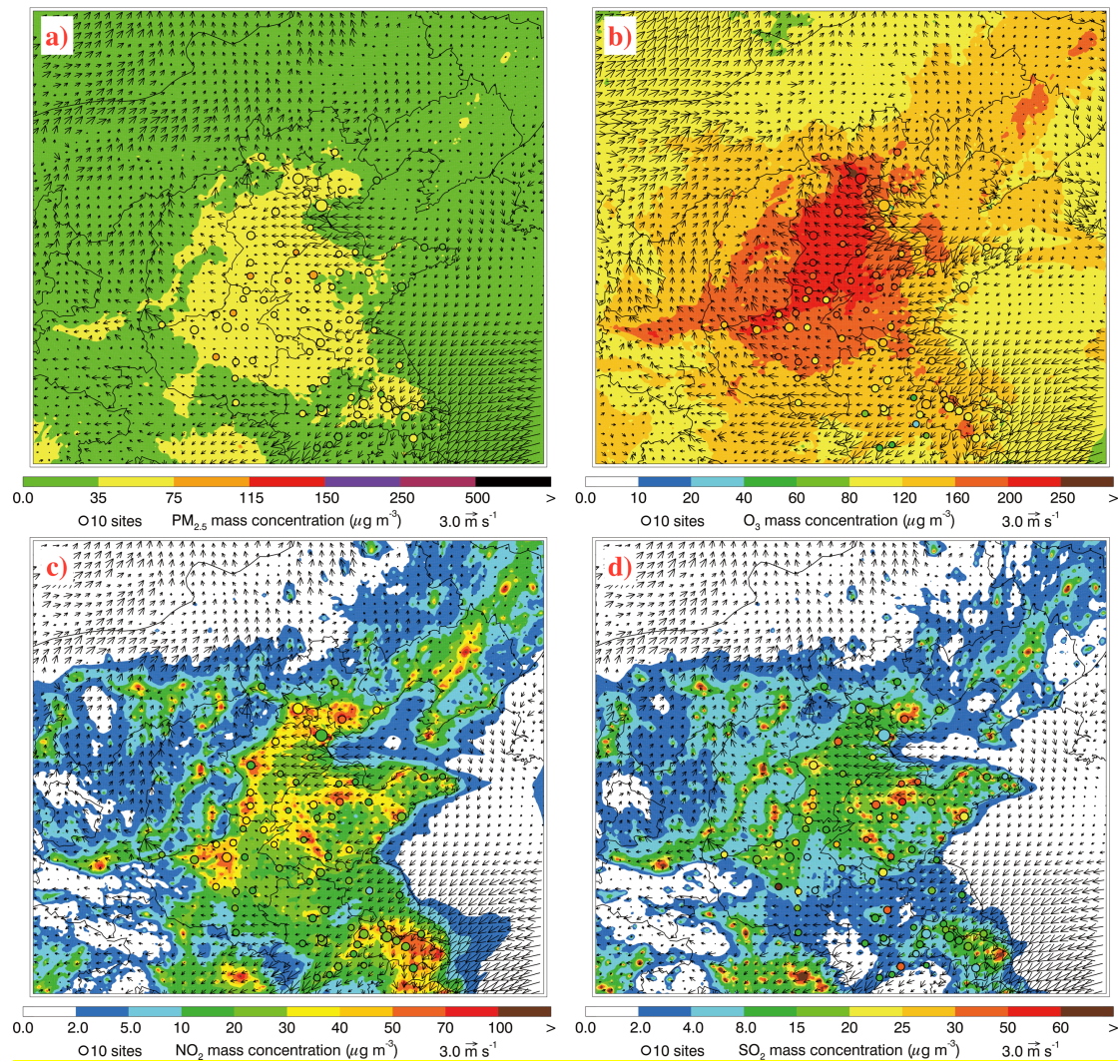
756
 757
 758
 759
 760
 761
 762
 763
 764
 765

Figure 2 Temporal variations of the simulated (blue line) and observed (black dots) near-surface (a) temperature, (b) relative humidity, (c) wind speed, and (d) wind direction at the weather station in Beijing from 04 to 15 July 2015.



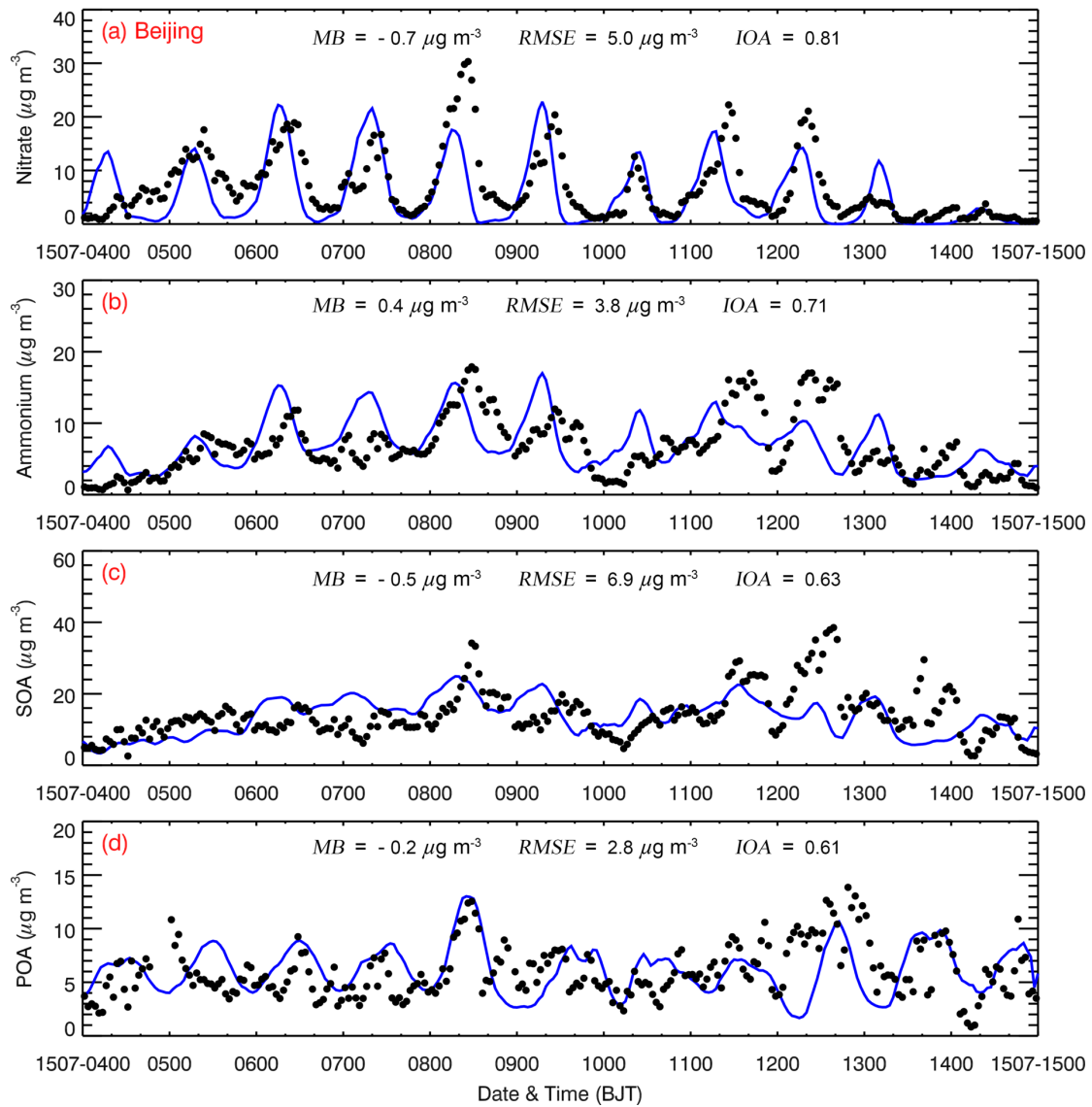
766
767
768
769
770
771
772
773
774
775

Figure 3 Comparison of observed (black dots) and simulated (blue line) diurnal profiles of near surface hourly (a) PM_{2.5}, (b) O₃, (c) NO₂, and (d) SO₂ averaged over all ambient monitoring stations in BTH from 04 to 15 July 2015.



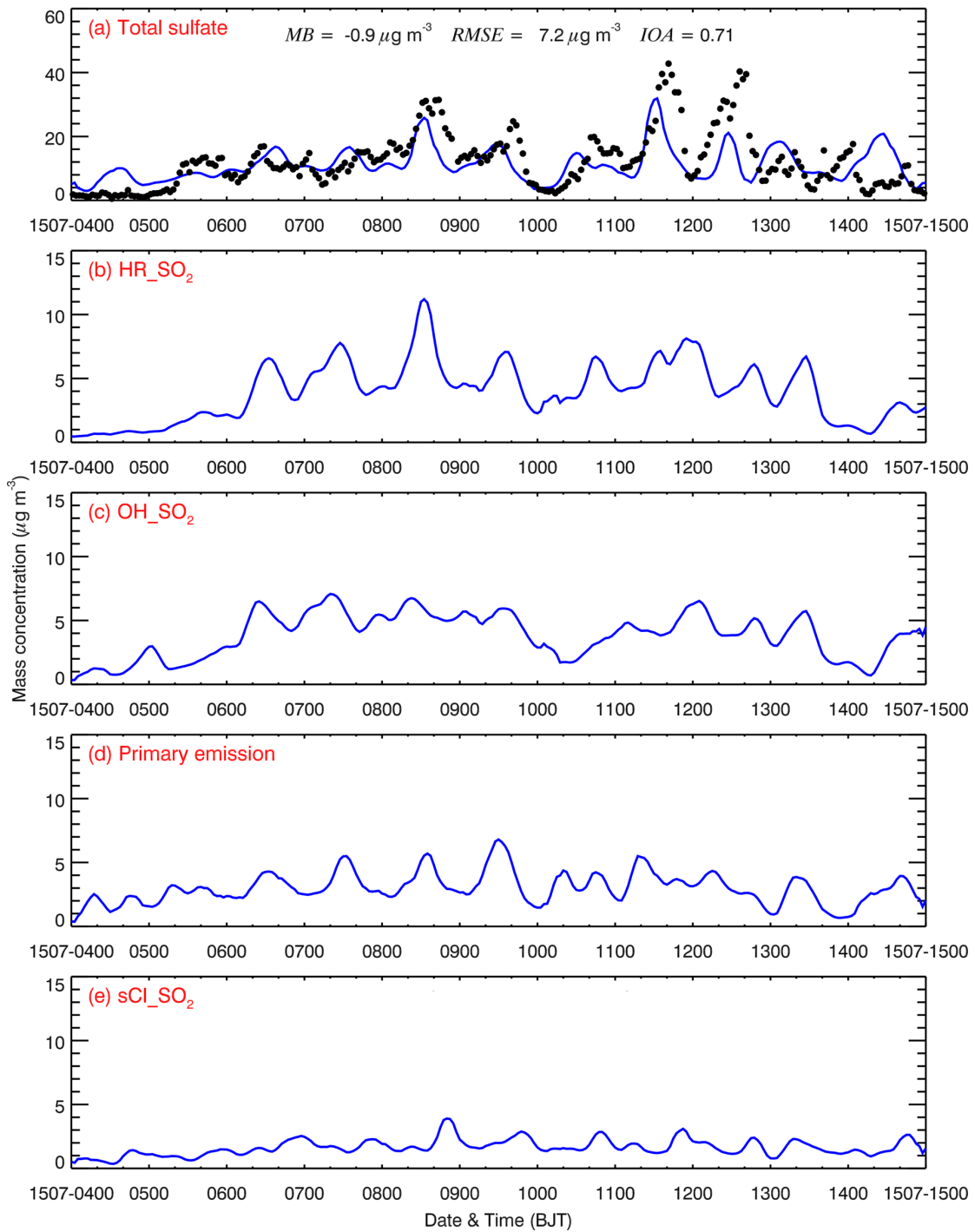
776
 777
 778
 779
 780
 781
 782
 783
 784
 785

Figure 4 Spatial distributions of average (a) PM_{2.5}, (b) peak O₃, (c) NO₂, and (d) SO₂ mass concentrations from 04 to 15 July 2015. Colored dots, colored contour, and black arrows are observations and simulations of air pollutants, and simulated surface winds, respectively.



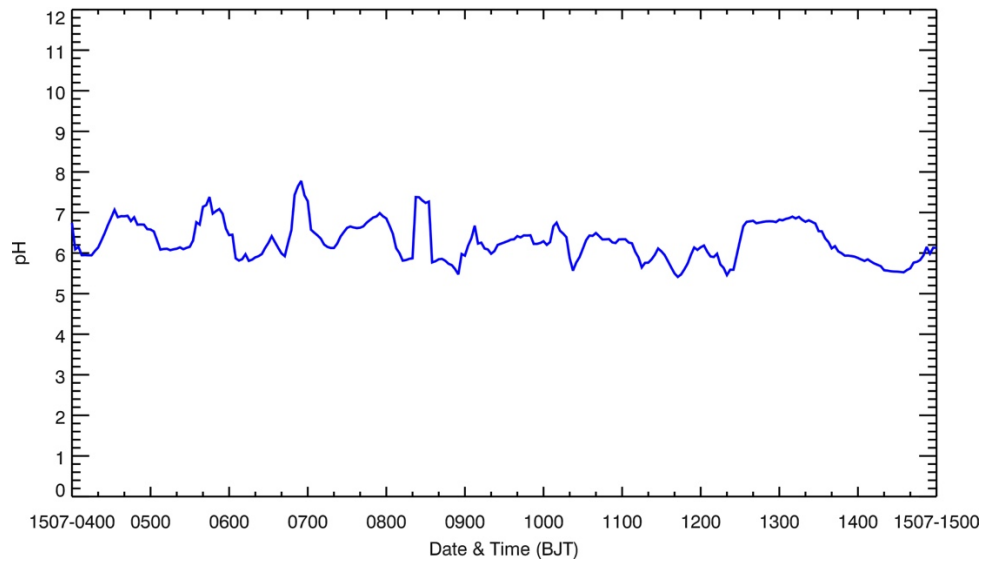
786
 787
 788
 789
 790
 791
 792
 793
 794
 795

Figure 5 Comparison of observed (black dots) and simulated (blue line) diurnal profiles of hourly submicron (a) nitrate, (b) ammonium, (c) SOA, and (d) POA mass concentrations at NCNST site in Beijing from 04 to 15 July 2015.



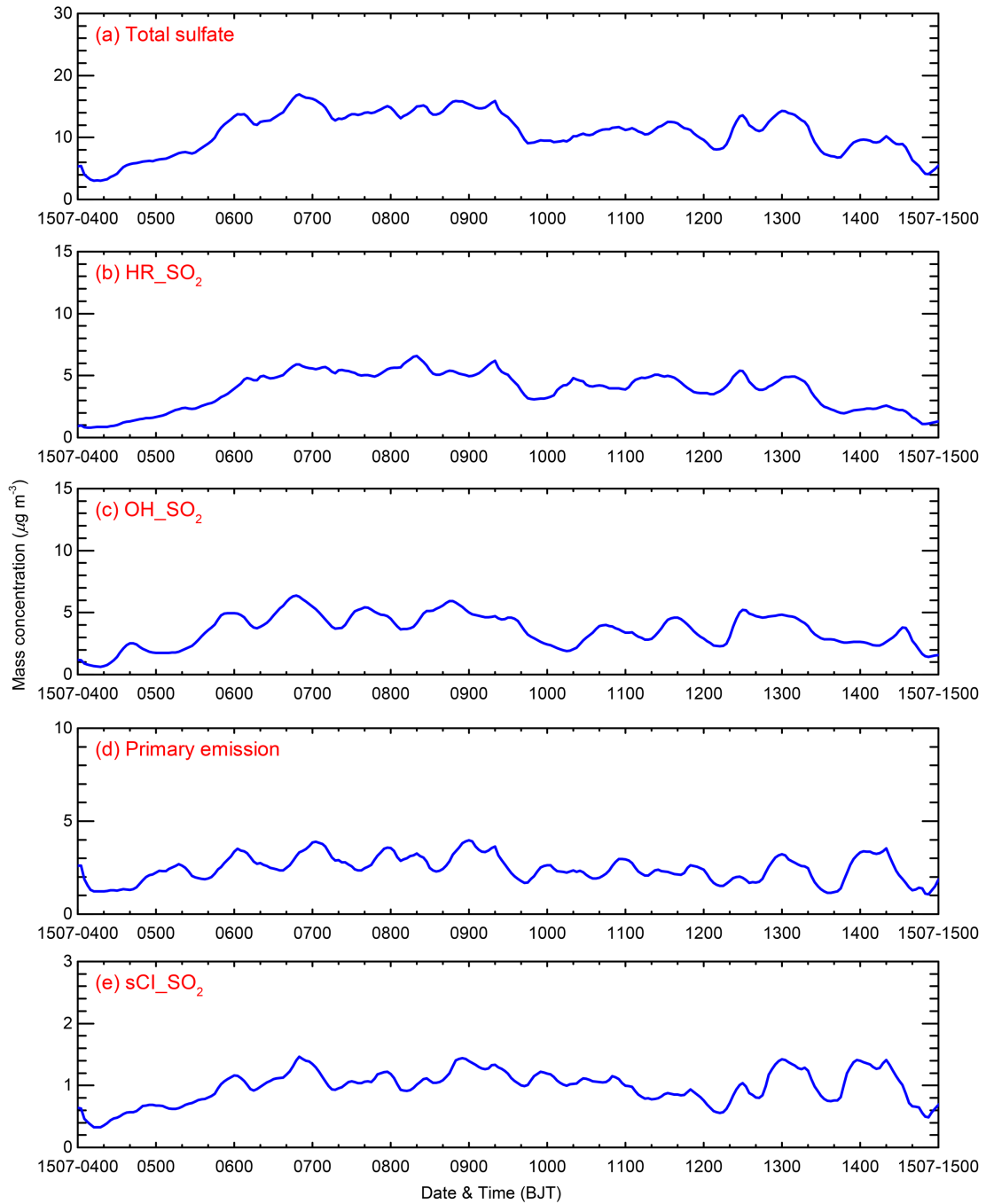
796
 797
 798
 799
 800
 801
 802
 803
 804
 805
 806

Figure 6 (a) Comparison of observed (black dots) and simulated (blue line) diurnal profiles of hourly submicron sulfate mass concentration, and temporal variation of simulated sulfate contribution of the (b) HR_{SO₂}, (c) OH_{SO₂}, (d) primary emission, and (e) sCl_{SO₂} to the sulfate concentration at NCNST site in Beijing from 04 to 15 July 2015.



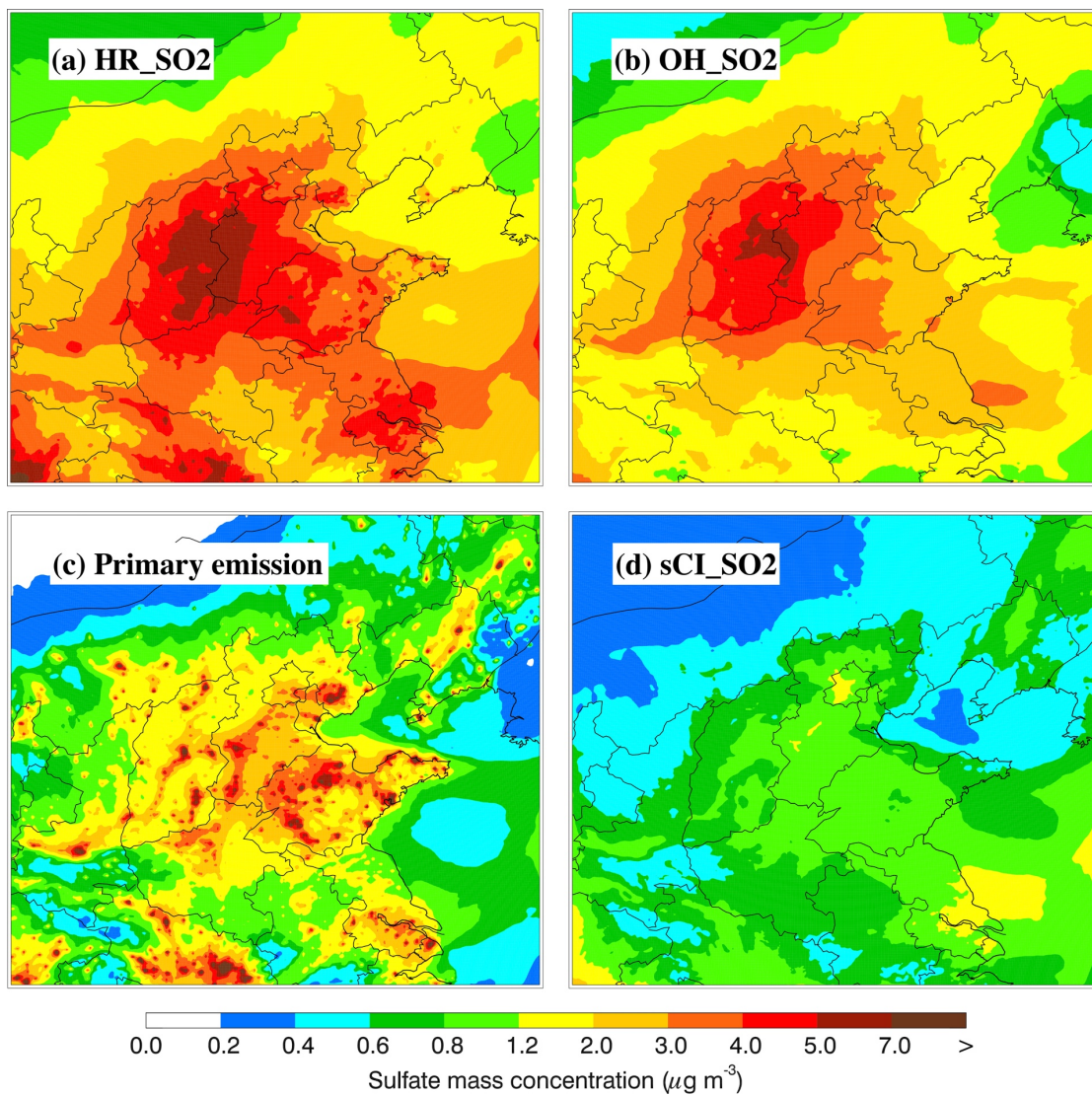
807
808
809
810
811
812
813
814

Figure 7 Temporal variation of the average simulated pH in Beijing from 04 to 15 July 2015.



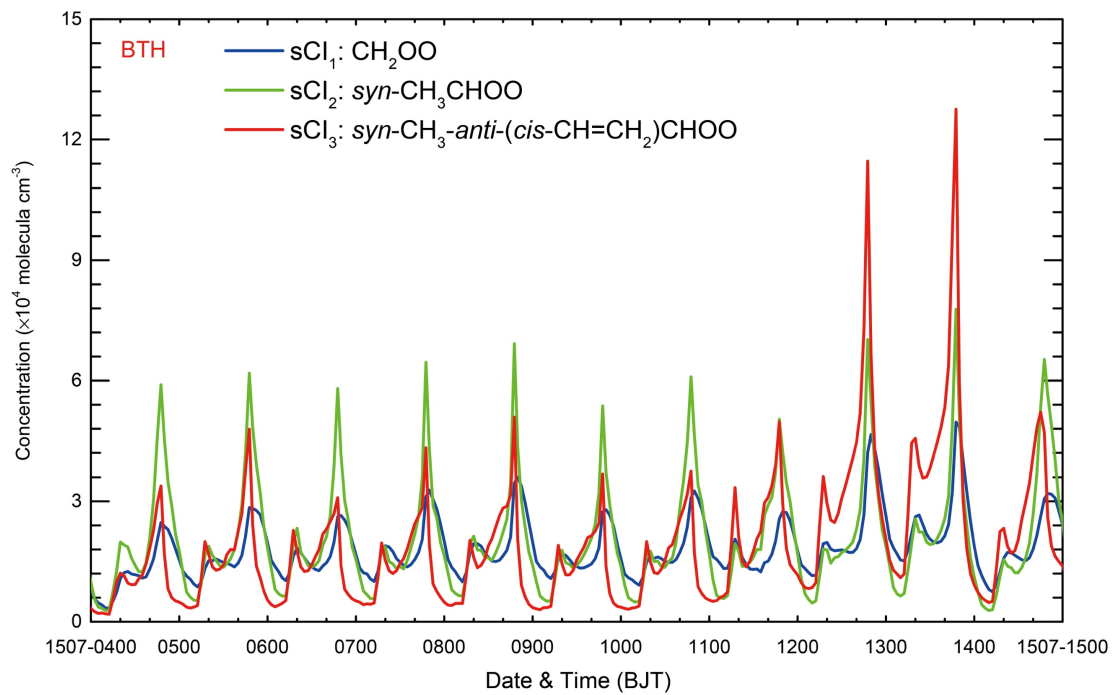
815
 816
 817
 818
 819
 820
 821

Figure 8 (a) Simulated diurnal profiles of total sulfate mass concentration, and contributions of the (b) HR_SO₂, (c) OH_SO₂, (d) primary emission, and (e) sCl_SO₂ to the sulfate concentration averaged over BTH from 04 to 15 July 2015.



823
824
825
826
827
828
829
830
831

Figure 9 Spatial distributions of average sulfate contributions of the (a) HR_SO₂, (b) OH_SO₂, (c) primary emission, and (d) sCl_SO₂ in BTH from 04 to 15 July 2015.



832

833

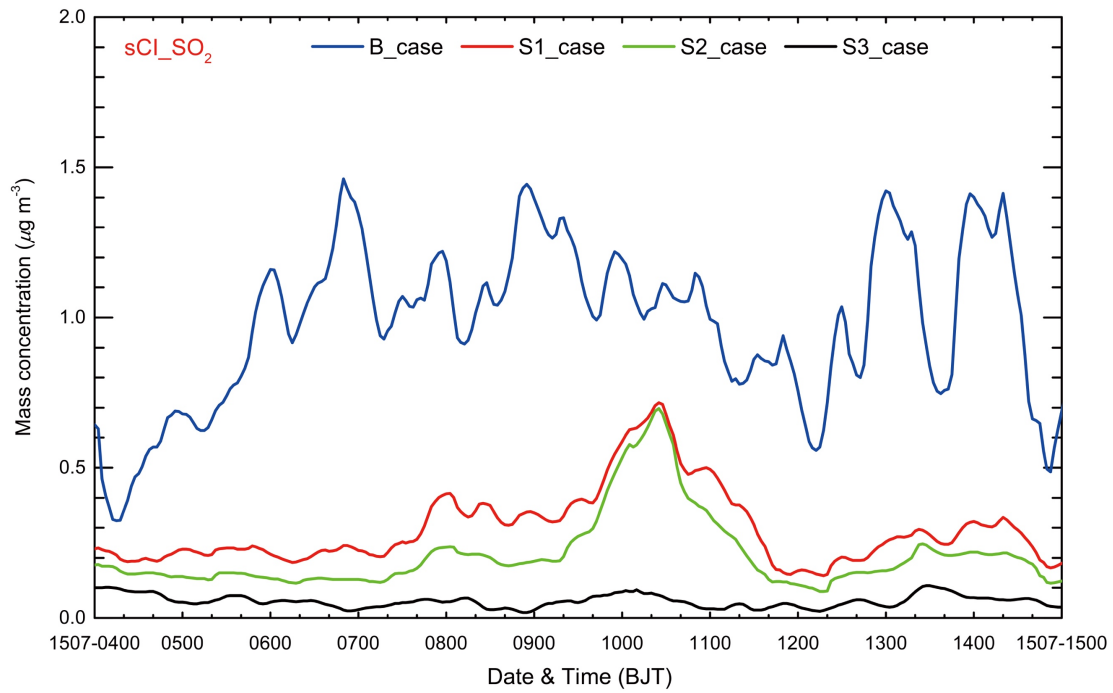
834 **Figure 10 Temporal variations of the simulated concentration of different sCI (Blue line: sCI₁;**

835 **Green line: sCI₂; Red line: sCI₃) in BTH from 04 to 15 July 2015.**

836

837

838



839

840

841 **Figure 11 Temporal variations of the simulated average sulfate concentration contributed by**
842 **the sCl₂/SO₂ (Blue line: B-case; Red line: S1-case; Green line: S2-case; Black line: S3-case)**
843 **in BTH from 04 to 15 July 2015.**

844

845

846

847